

國立臺灣大學工學院化學工程學研究所

碩士論文

Graduate Institute of Chemical Engineering

College of Engineering

National Taiwan University

Master Thesis



奈米孔道的離子電流整流：孔道形狀, pH 與鹽類性質的
影響

Ionic Current Rectification of Nanochannels: Effects of
Channel Geometry, pH, and Salt Conditions

林采葳

Tsai-Wei Lin

指導教授：徐治平 博士

Advisor: Jyh-Ping Hsu, Ph.D.

中華民國 108 年 6 月

June, 2019

誌謝



感謝恩師 徐治平教授從大學以來對我的指導與督促，無論是在研究上，或是待人上都使我受益良多，也謝謝口試委員曾琇瑱教授、張有義教授、游琇仔教授以及葉禮賢教授的指證與建議，使本論文能夠更臻完美。在 309 實驗室的這段期間，多虧有志原學長親自帶領我進行研究工作，給予我很多研究以及生活上的建議，讓我學到了很多很重要的研究態度與技能，志原學長無疑是我研究過程中的貴人。感謝淑端學姊、聖昌、尚宏、俞閔、育佑、子暉學長給予我的指導與幫助，使我的碩士生活充實且豐富。也非常感謝實驗室的學弟妹：偉誠、維寬、俊廷、宗諺、佳蓉，謝謝你們在我忙碌的時候分擔事務，與我討論研究內容。最要感謝的是我在 309 的好夥伴們：永哲和子喬，謝謝這兩年來的陪伴與幫助，謝謝你們和我一起處理實驗室的事務、討論研究方向。真心地希望並祝福大家都能找到自己所愛的地方，順利的生活。

感謝大學同學、雄友會同學、高中同學以及其他未具名的好友們，在我身邊陪伴我、傾聽我的想法，給我很多支持與建議。最後，感謝最重要的爸媽和姐姐，給予我最大的支持，尊重我所有的決定，讓我能夠專心地追求自己的夢想。

在此，僅將此論文獻給所有陪伴在我身邊的人們。

采葳

中文摘要



擁有高度應用潛力，奈米流體裝置近年來已受到須多研究團隊的重視。而為了提供給實驗團隊重要的結果以促進奈米流體裝置的實際應用，我們利用數值模擬研究這些奈米孔道中的離子傳輸行為。其中，離子電流整流行為為們主要研究對象。在第一章節中，我們探討許多因素對錐狀奈米孔道的電流整流行為的影響，囊括了孔道幾何與電解質濃度種類影響。在此研究中，我們討論的離子種類為：KCl、NaCl 及 LiCl。我們發現，當電解質濃度較低，且開口角度很小的奈米孔道中，LiCl 溶液有最佳的電流整流行為；然而，加大開口角度或是提高電解質濃度時，則是 KCl 的電流整流行為最佳。此研究成果已發表於 *Journal of Physical Chemistry C*。

第二章節中，利用表面塗佈有 pH 可調節聚電解質的圓柱狀奈米孔道，我們提出了同時施以外加電壓與外加酸鹼值 pH 梯度下，此奈米孔道的離子電流整流機制。我們觀察到，當施加較強的 pH 梯度，此圓柱狀奈米孔道的整流方向會隨著外加電壓大小而反轉；施加較弱的 pH 梯度，藉由提升聚電解質的接枝密度，可改變奈米孔道的整流方向。我們所提出的機制討論與研究結果已發表於 *Journal of Physical Chemistry C*。

關鍵字：奈米流體；離子電流整流；電導度；可調節聚電解質；酸鹼值梯度

Abstract



Nanofluidic devices have gained much attention for its applicability in many fields. To advance nanodevices' applications and provide significant results for experimental groups, we develop numerical models to simulate ion transport behaviors in nanopores. Ion current rectification (ICR) of nanopores is particularly focused in our studies. In the first part, the effects of nanopores' geometry, bulk salt concentration, and types of salt on ICR of conical nanopores are discussed in detail. Three types of salt are considered: KCl, NaCl, and LiCl. With sufficiently low salt concentration and small half cone angle, LiCl shows the best current rectifying behavior. The reverse of the trend is observed if we increases either the salt concentration or half cone angle. The above results was published in *Journal of Physical Chemistry C*.

In the second part, we provide a mechanism for ICR performance of a nanopore simultaneously applied with an electric potential and a pH gradient. A cylindrical nanopore functionalized with homogeneous (single) pH-tunable polyelectrolyte brushes is adopted in our study. We show that homogeneously modified nanopores can also exhibit ion current rectification behavior when applied an external pH gradient. The preferential direction of ionic current can be tuned by increasing level of applied electric potential if pH gradient is strong. For nanopores with weak pH gradient, an increase in grafting density of the polyelectrolyte chains can reverse preferential direction. The results and the discussion are published in *Journal of Physical Chemistry C*.

Keywords: Nanofluidic devices; Ion current rectification; Nanopore conductance; pH-tunable polyelectrolyte; pH gradient

List of Figures



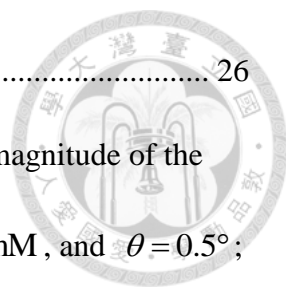
Figure 1-1. Schematic representation of the ion transport through a charged conical nanopore of tip radius R_{tip} , base radius R_{base} , and length L_n connecting two large, identical reservoirs filled with an aqueous salt solution. V_0 is the voltage bias applied across the nanopore with the electrode in the upper reservoir grounded. 22

Figure 1-2. Current-voltage curves for various salt solutions at various combinations of bulk salt concentration C_{bulk} and half cone angle θ at $R_{tip} = 6 \text{ nm}$. (a) $C_{bulk} = 3 \text{ mM}$ and $\theta = 0.5^\circ$; (b) $C_{bulk} = 3 \text{ mM}$ and $\theta = 1^\circ$; (c) $C_{bulk} = 3 \text{ mM}$ and $\theta = 5^\circ$; (d) $C_{bulk} = 100 \text{ mM}$ and $\theta = 1^\circ$ 23

Figure 1-3. Current rectification ratio, R_f , as a function of the magnitude of the applied voltage, $|V_0|$, for various salt solutions at various combinations of the bulk salt concentration C_{bulk} and the half cone angle θ at $R_{tip} = 6 \text{ nm}$. (a) $C_{bulk} = 3 \text{ mM}$ and $\theta = 0.5^\circ$; (b) $C_{bulk} = 3 \text{ mM}$ and $\theta = 1^\circ$; (c) $C_{bulk} = 3 \text{ mM}$ and $\theta = 5^\circ$; (d) $C_{bulk} = 100 \text{ mM}$ and $\theta = 1^\circ$ 24

Figure 1-4. Axial variations in the cross sectional averaged concentration difference ΔC_{avg} at $C_{bulk} = 3 \text{ mM}$ and $R_{tip} = 6 \text{ nm}$ for various combinations of the half cone angle θ and the applied voltage bias V_0 . (a) $\theta = 0.5^\circ$ and $V_0 = -0.5 \text{ V}$ (b) $\theta = 0.5^\circ$ and $V_0 = -1.5 \text{ V}$, (c) $\theta = 5^\circ$ and $V_0 = -0.5 \text{ V}$, (d) $\theta = 5^\circ$ and $V_0 = -1.5 \text{ V}$ 25

Figure 1-5. Axial variation of the cross sectional averaged electric potential at $V_0 = -1.5 \text{ V}$ and $R_{tip} = 6 \text{ nm}$ under various conditions. (a) $C_{bulk} = 3 \text{ mM}$ and $\theta = 1^\circ$;



(b) $C_{\text{bulk}} = 100 \text{ mM}$ and $\theta = 1^\circ$; (c) $C_{\text{bulk}} = 3 \text{ mM}$ and $\theta = 5^\circ$ 26

Figure 1-6. Variation of the current rectification ratio R_f with the magnitude of the applied voltage $|V_0|$ for various salts. (a): $R_{\text{tip}} = 6 \text{ nm}$, $C_{\text{bulk}} = 10 \text{ mM}$, and $\theta = 0.5^\circ$; (b): $R_{\text{tip}} = 15 \text{ nm}$, $C_{\text{bulk}} = 10 \text{ mM}$, and $\theta = 0.5^\circ$; (c): $R_{\text{tip}} = 30 \text{ nm}$, $C_{\text{bulk}} = 100 \text{ mM}$, and $\theta = 5^\circ$ 27

Figure 1-7. Variation of the ion selectivity S with the applied voltage bias V_0 at $R_{\text{tip}} = 6 \text{ nm}$ for various combinations of the type of salt and the half cone angle θ at $C_{\text{bulk}} = 3 \text{ mM}$, (a), and $C_{\text{bulk}} = 100 \text{ mM}$, (b)..... 28

Figure 1-8. Variation of $|J_i/V_0|$ with V_0 for two levels of C_{bulk} , where J_1 (J_2) is the cross sectional averaged flux of cations (anions) at $z=0$ for $\theta = 5^\circ$ and $R_{\text{tip}} = 6 \text{ nm}$. (a) and (b): $C_{\text{bulk}} = 3 \text{ mM}$; (c) and (d): $C_{\text{bulk}} = 100 \text{ mM}$ 29

Figure 1-S1. Variation of the conductance G with the bulk salt concentration C_{bulk} . Solid curve: bulk solution conductance; broken curve: analytic result at a constant surface charge density;⁵³ discrete symbols: present numerical result at $R_{\text{tip}}=6 \text{ nm}$, $R_{\text{base}}=93.49 \text{ nm}$, and $\sigma_s = -0.5 \text{ e/nm}^2$ 30

Figure 1-S2. Current rectification ratio R_f as a function of the half cone angle θ for an aqueous KCl solution at $R_{\text{tip}} = 6 \text{ nm}$ and $C_{\text{bulk}} = 100 \text{ mM}$ 31

Figure 1-S3. Current rectification ratio, R_f , as a function of the magnitude of the applied voltage, $|V_0|$, for various salt solutions at $R_{\text{tip}} = 6 \text{ nm}$ and $\theta = 1^\circ$. (a) $C_{\text{bulk}} = 300 \text{ mM}$; (b) $C_{\text{bulk}} = 1000 \text{ mM}$ 32

Figure 1-S4. Axial variations in the cross sectional averaged concentration difference ΔC_{avg} under various conditions, where $R_{\text{tip}} = 6 \text{ nm}$. (a) $C_{\text{bulk}} = 3 \text{ mM}$, $\theta = 0.5^\circ$, and

$V_0 = +0.5$ V (b) $C_{\text{bulk}} = 3$ mM, $\theta = 0.5^\circ$, and $V_0 = +1.5$ V, (c) $C_{\text{bulk}} = 3$ mM, $\theta = 5^\circ$, and $V_0 = +0.5$ V, (d) $C_{\text{bulk}} = 3$ mM, $\theta = 5^\circ$, and $V_0 = +1.5$ V 33

Figure 1-S5. Axial variations in the cross sectional averaged concentration difference

$\Delta C_{i,avg}$ under various conditions, where $R_{\text{tip}} = 6$ nm . (a) $C_{\text{bulk}} = 3$ mM, $\theta = 0.5^\circ$ and $V_0 = -0.5$ V (b) $C_{\text{bulk}} = 3$ mM, $\theta = 0.5^\circ$, and $V_0 = -1.5$ V, (c) $C_{\text{bulk}} = 3$ mM, $\theta = 5^\circ$, and $V_0 = -0.5$ V, (d) $C_{\text{bulk}} = 3$ mM, $\theta = 5^\circ$, and $V_0 = -1.5$ V . Curves: cations; discrete symbols: anions. 34

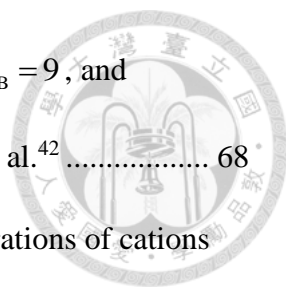
Figure 1-S6. Axial variations of the electric potential ϕ at $V_0 = +1.5$ V under various conditions, where $R_{\text{tip}} = 6$ nm (a) $C_{\text{bulk}} = 3$ mM and $\theta = 1^\circ$; (b) $C_{\text{bulk}} = 100$ mM and $\theta = 1^\circ$; (c) $C_{\text{bulk}} = 3$ mM and $\theta = 5^\circ$ 35

Figure 1-S7. Current rectification ratio, R_f , as a function of the magnitude of the applied voltage, $|V_0|$, for various salt solutions at $R_{\text{tip}} = 3$ nm . (a) $C_{\text{bulk}} = 3$ mM and $\theta = 0.5^\circ$; (b) $C_{\text{bulk}} = 100$ mM and $\theta = 1^\circ$ 36

Figure 1-S8. Ionic current-voltage curves for various electrolyte solutions at various combination of salt concentration C_{bulk} and half cone angle θ , where $R_{\text{tip}} = 6$ nm . (a) $C_{\text{bulk}} = 3$ mM and $\theta = 5^\circ$; (b) $C_{\text{bulk}} = 100$ mM and $\theta = 5^\circ$ 37

Figure 1-S9. Variation of the selectivity S with the applied voltage bias V_0 when $R_{\text{tip}} = 6$ nm for various combinations of the type of salt and the half cone angle θ at $C_{\text{bulk}} = 3$ mM, (a), and $C_{\text{bulk}} = 100$ mM, (b). 38

Figure 2-S1. Current-voltage curves of a single polyethylene terephthalate (PET) conical nanopore with its surface functionalized with Lysine in 100 mM KCl solution for various pH values. The pore thickness is 12 μm with tip radius of 8 nm and base radius of 165 nm. The polyelectrolyte layer is assumed 1 nm thick with $\lambda = 0.2$ nm.²⁷,



⁵⁷ Curves: present theoretical results with variables $pK_A = 2.2$, $pK_B = 9$, and $N_{total} = 0.6$ chains/nm²; discrete symbols: experimental data of Ali et al.⁴² 68

Figure 2-S2. Axial variation in the cross sectional averaged concentrations of cations (K⁺ and H⁺) and anions (Cl⁻ and OH⁻) with $N_{total} = 0.1$ chains/nm² at pH_H/pH_L=11/3, (a), and pH_H/pH_L=7/3, (b). Curves: $V_{applied} = 0.2$ V; discrete symbols: $V_{applied} = 0.5$ V .69

Figure 2-S3. Concentration profiles of K⁺, (a) and (b), and Cl⁻, (c) and (d), for two values of the grafting density of PE chains N_{total} at pH_H/pH_L=11/3. 70

Figure 2-S4. Axial variation in the charge density of the PE layer ρ_m for various levels of $V_{applied}$ with $N_{total} = 0.5$ chains/nm² at pH_H/pH_L=11/3, (a), and pH_H/pH_L=7/3, (b). 71

Figure 2-S5. Concentration profiles of H⁺ for two values of grafting density of PE chains N_{total} at pH_H/pH_L=7/3. 72

Figure 2-S6. Concentration profiles of K⁺, (a) and (b), and Cl⁻, (c) and (d), for two values of the grafting density of PE chains N_{total} at pH_H/pH_L=7/3. 73

Figure 2-S1. Current-voltage curves of a single polyethylene terephthalate (PET) conical nanopore with its surface functionalized with Lysine in 100 mM KCl solution for various pH values. The pore thickness is 12 μm with tip radius of 8 nm and base radius of 165 nm. The polyelectrolyte layer is assumed 1 nm thick with $\lambda = 0.2$ nm.²⁷,

⁵⁷ Curves: present theoretical results with variables $pK_A = 2.2$, $pK_B = 9$, and $N_{total} = 0.6$ chains/nm²; discrete symbols: experimental data of Ali et al.⁴² 68

Figure 2-S2. Axial variation in the cross sectional averaged concentrations of cations (K⁺ and H⁺) and anions (Cl⁻ and OH⁻) with $N_{total} = 0.1$ chains/nm² at pH_H/pH_L=11/3, (a), and pH_H/pH_L=7/3, (b). Curves: $V_{applied} = 0.2$ V; discrete symbols: $V_{applied} = 0.5$ V .69

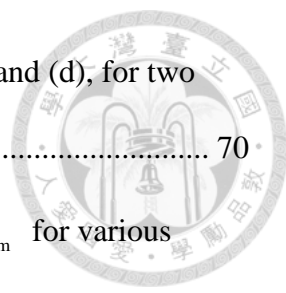


Figure 2-S3. Concentration profiles of K^+ , (a) and (b), and Cl^- , (c) and (d), for two values of the grafting density of PE chains N_{total} at $pH_H/pH_L=11/3$ 70

Figure 2-S4. Axial variation in the charge density of the PE layer ρ_m for various levels of $V_{applied}$ with $N_{total} = 0.5$ chains/nm² at $pH_H/pH_L=11/3$, (a), and $pH_H/pH_L=7/3$, (b). 71

Figure 2-S5. Concentration profiles of H^+ for two values of grafting density of PE chains N_{total} at $pH_H/pH_L=7/3$ 72

Figure 2-S6. Concentration profiles of K^+ , (a) and (b), and Cl^- , (c) and (d), for two values of the grafting density of PE chains N_{total} at $pH_H/pH_L=7/3$ 73

List of Tables

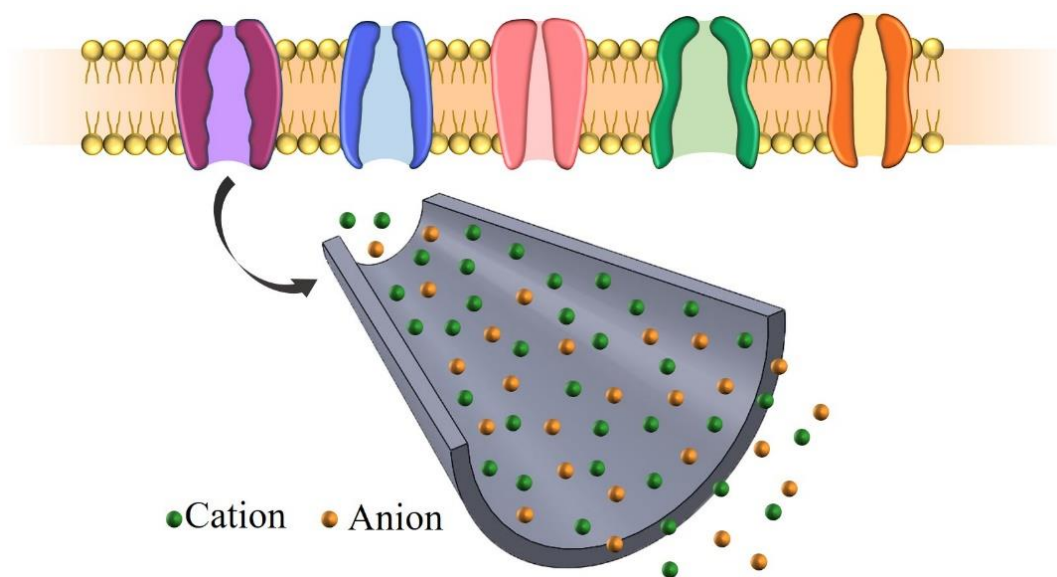


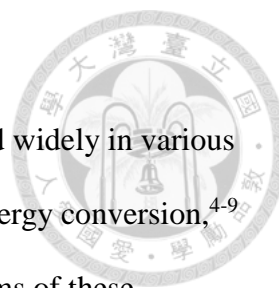
Table 1-1. Summary of the boundary conditions assumed	21
Table 2-1. Boundary conditions assumed for eqs 1-4.....	61



Chapter 1 Salt Dependent Ion Current Rectification in Conical

Nanopores: Impact of Salt Concentration and Cone Angle



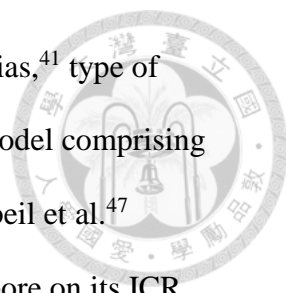


1-1. Introduction

Recently, nanopore/nanochannel based devices have been applied widely in various areas of practical significance, including, for example, ion gate,¹⁻³ energy conversion,⁴⁻⁹ DNA translocation,¹⁰⁻¹² and biosensor.¹³⁻¹⁶ The underlying mechanisms of these applications are electric double layer (EDL) overlapping¹⁷⁻¹⁹ and associated specific ionic transport behaviors. The former arises from that the linear size of a device (e.g., nanopore radius) can be on the order of EDL thickness, yielding profound and interesting electrokinetic phenomena. These include, for instance, ion concentration polarization (ICP),^{18, 20-21} ion selectivity,²²⁻²³ and ionic current rectification (ICR).²⁴⁻²⁵ ICP refers to the asymmetric distribution of ions across a nanopore when an electric potential bias is applied. Ion selectivity stems from that a charged nanopore attracts counterions and repels coions simultaneously so that either cations or anions are easier to pass through than the other. ICR denotes the preference of the ionic current direction when a potential bias is applied. This specific behavior can be attributed to the asymmetric nanopore geometry,²⁶⁻²⁷ asymmetric surface charge distribution,²⁸⁻³¹ wettability difference,³²⁻³³ and external stimuli.³⁴⁻³⁵

The application of a potential bias across a charged nanopore/nanochannel yields an electroosmotic flow (EOF).³⁶⁻³⁷ Although this effect is often neglected in previous studies, for simplicity, it can play an important role in relevant electrokinetic phenomena. For instance, Ai et al.³⁸ showed that if the surface charge density is fixed, the influence of EOF on the ICR behavior of a conical nanopore is significant if its EDL is medium thick and the applied voltage bias sufficiently high. Their analysis was extended by Lin et al.³⁹ to the case of a conical nanopore having a charge-regulated surface.

Several factors have been proposed for explaining the ICR behavior of a nanopore,



including, for example, surface charge density,^{38,40} applied voltage bias,⁴¹ type of ions,⁴²⁻⁴⁴ salt gradient,⁴⁵⁻⁴⁶ and nanopore geometry.⁴⁷⁻⁵⁰ Adopting a model comprising Poisson-Nernst-Planck (PNP) equations (i.e., EOF is neglected), Kubeil et al.⁴⁷ examined the influences of the radius and the angle of a conical nanopore on its ICR behavior. Assuming a fixed surface charge density, they showed that these influences can be important. Tseng et al.⁴⁹ extended their study by considering a model comprising PNP and Navier-Stokes (PNP+NS) equations, where both the tip-end and the base-end radii are subject to change. It was concluded that the EOF effect can be significant.

Another factor which can be of practical significance is the presence of multivalent ions in the liquid phase. The influence of this factor on the ICR behavior of a nanopore/nanochannel was studied both theoretically and experimentally. Pérez-Mitta et al.⁴⁴ illustrated that both the ionic current and the rectification efficiency of K_2SO_4 are larger than those of KCl. For aqueous, alkali chloride salt solutions in an α -hemolysin modified nanopore, Bhattacharya et al.⁵¹ showed experimentally that the ICR ratio of various monovalent salts ranks as $LiCl < NaCl < KCl < RbCl < CsCl$. Gamble et al.⁴³ examined experimentally the type of ion species on the ICR behavior of a conical PET nanopore. Through molecular dynamics simulation, they proposed that the effective surface charge of a PET nanopore depends upon the degree of binding of ions with the carboxyl groups on its wall. The result obtained was used to explain the dependence of the ICR behavior of a nanopore on the types of salt predicted by a PNP model. Hsu et al.⁴² showed that this dependence can also be attributed to the presence of EOF. Considering a conical nanopore, Cao et al.⁷ concluded that the performance of reverse electro dialysis depends highly upon the composition of the electrolyte solution. For instance, the salinity power generated from cation-selective (anion-selective) nanopores increases (decreases) with the cation mobility. It was also shown that the ionic species

dependence of ICR could be tuned through applying a concentration gradient.⁴⁶

Up to now, the influence of the nanopore geometry on its ionic current rectification behavior taking account of both type of salt and EOF has not been discussed comprehensively. This is conducted in the present study by considering conical nanopores having a fixed charge density. The influence of the nanopore geometry is investigated by varying the cone angle and the tip-end radius. Three typical types of monovalent salt are examined: KCl, NaCl, and LiCl.

1-2. Theoretical model

As illustrated in Figure 1-1, we consider a conical nanopore of the tip radius R_{tip} , base radius R_{base} , and axial length L_n connecting two identical, cylindrical reservoirs filled with an aqueous salt solution. The length and the radius of the reservoirs are sufficiently large so that the salt concentration at a point far away from the nanopore reaches essentially the bulk value. The ionic species is driven from one reservoir through the nanopore to the other by a potential bias V_0 applied across the nanopore. The two electrodes are positioned in the reservoirs located far away from the nanopore where the electrode in the upper reservoir is grounded. The cylindrical coordinates with the origin at the center of the nanopore tip are adopted. However, since the present problem is axial symmetric, only the (r, z) domain needs be considered, r and z being the radial and the axial coordinates, respectively.

The transport of ionic species in the system under consideration can be described by Poisson-Nernst-Planck equation

$$\nabla \cdot \mathbf{N}_i = \nabla \cdot \left(\mathbf{u}c_i - D_i \nabla c_i - z_i \frac{D_i}{RT} F c_i \nabla \phi \right) = 0, \quad (1)$$

where the electric potential ϕ is governed by Poisson equation

$$-\varepsilon_f \nabla^2 \phi = F \sum_{i=1}^2 z_i c_i \quad (2)$$

In these expressions, $\mathbf{u} = u\mathbf{e}_r + v\mathbf{e}_z$ is the fluid velocity with \mathbf{e}_r and \mathbf{e}_z being the unit vectors in the r and z directions, respectively, and u and v the corresponding velocity components. \mathbf{N}_i , c_i , D_i , and z_i are the flux, concentration, diffusivity, and valence of the i th ionic species, respectively (i is 1 for cations and 2 for anions). ε_f , F , R , and T are the fluid permittivity, Faraday constant, gas constant, and the absolute temperature, respectively.

Since the Reynolds number is small in our system, the fluid velocity can be determined from the equation of continuity and the modified Navier-Stokes equations

$$\nabla \cdot \mathbf{u} = 0 \quad (3)$$

$$-\nabla p + \mu \nabla^2 \mathbf{u} - F \sum_{i=1}^2 z_i c_i \nabla \phi = \mathbf{0} \quad (4)$$

p and μ are the hydrodynamic pressure and the fluid viscosity, respectively. Considering these equations implies that the effect of electroosmotic flow (EOF) is taken into account.

To specify the boundary conditions associated with Eqs. (1)-(4), we assume the following. (i) The nanopore walls (surfaces 4, 5, and 6, see table below) are ion-impenetrable ($\mathbf{n} \cdot \mathbf{N}_i = 0$), nonslip ($\mathbf{u} = \mathbf{0}$), and have the charge density σ_s ($-\varepsilon_f \mathbf{n} \cdot \nabla \phi = \sigma_s$). Here, we assume that the deprotonation of the functional groups of the nanopore material is complete so that σ_s is constant.⁵² (ii) The side boundaries of the two reservoirs (surfaces 3 and 7) have zero normal flux ($\mathbf{n} \cdot \mathbf{N}_i = 0$), are charge free ($-\mathbf{n} \cdot \nabla \phi = 0$), and slip. (iii) The end surfaces 2 and 8 are sufficiently far from the nanopore, where surface 2 in the top reservoir is grounded ($\phi = 0$), and a voltage bias ($\phi = V_0$) is applied to surface 8 in the bottom reservoir. (iv) The ionic concentrations on

surfaces 2 and 8 reach essentially the bulk value ($c_i = C_{\text{bulk}}$). These are summarized in the table below.

Letting S be a surface normal to the nanopore axis, the ionic current I through the nanopore can be evaluated by

$$I = \int_S F \left(\sum_{i=1}^2 z_i \mathbf{N}_i \right) \cdot \mathbf{n} dS \quad (5)$$

1-3. Results and discussion

Equations (1)-(4) and the associated boundary conditions are solved numerically by COMSOL (version 4.3a, <http://www.comsol.com>) operated in a high-performance cluster. The applicability of the numerical scheme adopted is verified by Figure 1-S1. To examine the behavior of the system under consideration, a thorough numerical simulation is conducted. For illustration, we assume the following: $L_n=5000$ nm, $\sigma_s = -0.5$ e/nm², $F=96485$ C/mol, $R=8.314$ J/mol·K, $T=298$ K, $\mu=0.001$ Pa·s, $\epsilon_f = 6.95 \times 10^{-10}$ F/m, $D_1(\text{K}^+) = 1.96 \times 10^{-9}$ m²/s, $D_1(\text{Na}^+) = 1.33 \times 10^{-9}$ m²/s, $D_1(\text{Li}^+) = 1.03 \times 10^{-9}$ m²/s, and $D_2(\text{Cl}^-) = 2.03 \times 10^{-9}$ m²/s. The influences of the half cone angle θ , the bulk salt concentration C_{bulk} , the applied voltage bias V_0 , the nanopore tip radius R_{tip} , and the type of salt (KCl, NaCl, LiCl) on the current rectification behavior of the nanopore are examined in subsequent discussion. The degree of current rectification is measured by the rectification ratio $R_f = [I(-V)/I(V)]$.⁴³ According to previous studies,^{16, 49} the degree of R_f shows a local maximum with varying cone angle, as depicted in Figure 1-S2. Since R_f has a maximum at a cone angle close to 1° (or $2\theta \cong 1^\circ \sim 2^\circ$, θ is the half cone angle in our study), we assumed that

$0.5^\circ \leq \theta \leq 5^\circ$ in the numerical simulation so that the optimum cone angle could be included.



1-3-1 Current-voltage curves

The results illustrated in Figure 1-2 reveal that $I(V_0 < 0)$ is larger than the corresponding $I(V_0 > 0)$. This preference in the current direction is known as ion current rectification (ICR), which can be explained by the enrichment/depletion of the ions in a nanopore caused by the difference in ionic fluxes inside/outside it. Figure 1-2 also reveals that, regardless of the sign of V_0 , the magnitude of I for the types of salt considered ranks as $|I(\text{KCl})| > |I(\text{NaCl})| > |I(\text{LiCl})|$, which can be attributed to the relative magnitudes in the cationic diffusivities. In addition, the magnitude of I increases with increasing C_{bulk} or θ . The former is expected because the higher the bulk salt concentration the larger the amounts of cations and anions driven through the nanopore. The latter is due to the fact that the surface area, and therefore, the effective cross sectional area of the nanopore increases with increasing cone angle.

1-3-2 Current rectification

Figure 1-3(a) shows that at $C_{\text{bulk}} = 3 \text{ mM}$ and $\theta = 0.5^\circ$, the value of R_f for various types of salt ranks as $R_f(\text{LiCl}) > R_f(\text{NaCl}) > R_f(\text{KCl})$. However, if θ is raised to 1° , this order is reversed when $|V_0|$ is sufficiently high, as seen in Figure 1-3(b). This makes the $R_f - |V_0|$ curves of the salts examined intersect at the same point.⁴²⁻⁴³ As seen in Figure 1-3(c), if θ is further raised to 5° , the value of $|V_0|$ at which the intersection of the $R_f - |V_0|$ curves occur becomes smaller; that is, the reverse in the order of R_f occurs at a lower applied voltage bias. A comparison between Figure

1-3(b) and 3(d) reveals that if θ is fixed, raising the level of C_{bulk} also makes that intersection to occur at a lower level of $|V_0|$. As will be discussed later, these phenomena can be attributed to a decrease in the degree of double layer overlapping inside the nanopore as θ and/or C_{bulk} are raised. Note that, as shown in Figure 1-S3, the qualitative ICR behaviors at higher salt concentration (e.g. 300 mM and 1000 mM) are essentially the same as those at 100 mM.

The order of R_f for various types of salt observed in Figure 1-3 can be explained by the variation in the distribution of ions in the nanopore with the applied voltage bias. In the absence of V_0 , cations (counterions) are attracted into the negatively charged nanopore. The application of V_0 influences the distribution of ions, leading to either an enrichment or a depletion of the ions in the nanopore. Figure 1-4 illustrates the difference in the ionic concentration, $\Delta C_{\text{avg}} = (\bar{c}_1 - \bar{c}_1^0) + (\bar{c}_2 - \bar{c}_2^0)$, caused by a negative applied voltage bias under various conditions. That by a positive applied voltage bias is shown in Figure 1-S4. \bar{c}_i is the cross sectional averaged concentration of the i th ionic species, and \bar{c}_i^0 denotes its value at $V_0=0$ V. As seen in Figure 1-S4, the value of ΔC_{avg} for $V_0>0$ is insensitive to the type of salt, implying that the species-dependent ICR behavior observed previously arises mainly from the ionic transport for $V_0<0$. As shown in Figure 1-4(a) and 1-4(c), if the negative applied voltage bias is low ($V_0 = -0.5$ V), the degree of ion enrichment follows the order $\text{LiCl}>\text{NaCl}>\text{KCl}$, which is consistent with that of R_f . On the other hand, if the negative applied voltage bias is high ($V_0 = -1.5$ V), the order of the degree of ion enrichment remains the same at $\theta = 0.5^\circ$, but becomes reversed (i.e., $\text{KCl}>\text{NaCl}>\text{LiCl}$)

at $\theta = 5^\circ$. This explains the behavior of the $R_f - |V_0|$ curves seen in Figure 1-3(a) and 3(c).

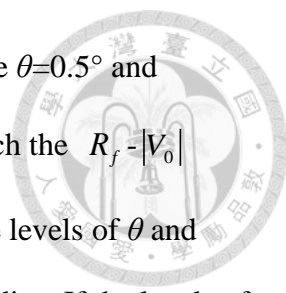


1-3-3 Axial variation in cross sectional averaged potential

The axial variation in the cross sectional averaged electric potential at $V_0 = -1.5$ V for various combinations of the values of θ and C_{bulk} is presented in Figure 1-5. Since the nanopore is negatively charged (i.e., cation-selective), the total amount of cations driven by a negative applied voltage bias into it is greater than that of anions. The more the amount of cations accumulated near the nanopore tip the slower the rate of decrease in the electric potential. Figure 1-5(a) shows that the rate of decrease in the electric potential drop at $C_{\text{bulk}} = 3$ mM and $\theta = 1^\circ$ ranks as $\text{LiCl} > \text{NaCl} > \text{KCl}$. This implies that KCl accumulates more inside the nanopore than other salts, yielding a slower potential drop. However, if C_{bulk} (Figure 1-5(b)) or θ (Figure 1-5(c)) takes a higher value, the degree of EDL overlapping decreases, and ions accumulate mostly near the nanopore tip. In this case, the difference in the distribution of electric potential among the types of salt considered is insignificant, and the rate of ion transport is dominated by the diffusivity of cations, which ranks as $D_{\text{K}^+} > D_{\text{Na}^+} > D_{\text{Li}^+}$, so that the associated R_f follows the same order. This reasonably explains the observed voltage-dependent ICR behaviors of the types of salt examined in Figure 1- 3. The corresponding distributions of the electric potential at $V_0 = 1.5$ V are plotted in Figure 1-S6, which shows that the electric potential is influenced by C_{bulk} , θ , and the type of salt.

1-3-4 Influence of tip radius

The influence of the tip radius of a nanopore R_{tip} on its current rectification behavior



is illustrated in Figure 1-6. As seen in Figure 1-6(a) and 1-6(b), where $\theta=0.5^\circ$ and $C_{\text{bulk}}=10 \text{ mM}$, the larger the R_{tip} the smaller the value of $|V_0|$ at which the $R_f - |V_0|$ curves of the types of salt intersect. This is because that, for the same levels of θ and C_{bulk} , the region of EDL overlapping decreases with increasing tip radius. If the levels of θ , C_{bulk} , and R_{tip} are all raised to those of Figure 1-6(c), the magnitude of R_f ranks as $R_f(\text{KCl}) > R_f(\text{NaCl}) > R_f(\text{LiCl})$ for all the levels of V_0 applied. This is because the EDL is thin in this case, so that the region of EDL overlapping reduces considerably and, therefore, R_f is mainly dominated by the diffusivity of cations. Figure 1-6(c) also reveals that R_f has a local maximum as $|V_0|$ varies. As mentioned previously, the enrichment and depletion of ions in a charged nanopore exhibiting ICR behavior can be attributed to the difference in the ionic fluxes inside/outside it. However, if EDL is thin, the ionic fluxes inside/outside the nanopore are comparable, especially when the applied voltage bias is high, so that R_f decreases. On the other hand, the current rectification behaviors for tip radius smaller than 6 nm is shown in Figure 1-S7. Compared with Figure 1-3(a) and Figure 1-3(d), the behaviors of R_f for $R_{\text{tip}} = 3 \text{ nm}$ are similar to those for $R_{\text{tip}} = 6 \text{ nm}$, implying that a lower R_{tip} will not influence the qualitative ICR behavior under the present conditions.

1-3-5 Ion selectivity for $V_0 < 0$

Figure 1-7 shows the influences of the half cone angle θ and the applied voltage bias V_0 on the selectivity of the nanopore, $S = \frac{|I_{\text{cation}}| - |I_{\text{anion}}|}{|I_{\text{cation}}| + |I_{\text{anion}}|}$, for various types of salt. If $S > 0$ ($S < 0$), the nanopore is cation-selective (anion-selective). In our case, because the nanopore is negatively charged, the ions driven through it are mainly cations (i.e.,

cation-selective). Figure 1-7 reveals that the magnitude of S ranks as

$S(\text{KCl}) > S(\text{NaCl}) > S(\text{LiCl})$. As seen in Figure 1-S8, the level of the difference

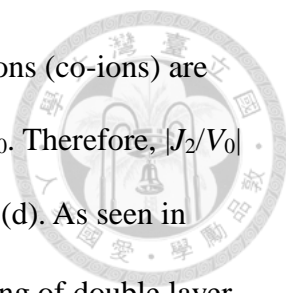
between I_{cation} and I_{anion} follows the order $\text{KCl} > \text{NaCl} > \text{LiCl}$, implying that the

contribution of cations to ionic current ranks as $\text{K}^+ > \text{Na}^+ > \text{Li}^+$. This explains the

observed order of S for the types of salt examined.

As can be seen in Figure 1-7(a), at $C_{\text{bulk}} = 3 \text{ mM}$ and $\theta = 0.5^\circ$, the selectivity of all the types of salt examined is close to unity, implying that the nanopore is highly cation-selective. This figure also indicates that S decreases significantly as θ increases, which is expected since the degree of double layer overlapping in the nanopore decreases with increasing θ . In addition, S decreases with increasing V_0 . This is because the larger the V_0 the more significant the ion enrichment inside the nanopore so that the less significant the overlapping of double layer, leading to a smaller S . Figure 1-7(b) shows that the S at $C_{\text{bulk}} = 100 \text{ mM}$ is smaller than that at $C_{\text{bulk}} = 3 \text{ mM}$. Again, this is due to a less significant double layer overlapping in the former.

Interestingly, the S at $\theta = 5^\circ$ does not decrease monotonically with increasing V_0 as that observed at $\theta = 0.5^\circ$, and the S of LiCl at $\theta = 5^\circ$ is larger than that at $\theta = 0.5^\circ$ for $-1 \text{ V} < V_0 < -0.7 \text{ V}$. These anomalous behaviors can be explained by the ionic flux near the nanopore tip shown in Figure 1-8, where J_1 (J_2) is the cross sectional averaged flux of cations (anions). At $C_{\text{bulk}} = 3 \text{ mM}$, the significantly overlapped double layer yields an induced electric field near the nanopore tip with its direction opposite to that of V_0 so that V_0 is lessened. Figure 1-8(a) shows that $|J_1/V_0|$ decreases with increasing V_0 until V_0 is sufficiently large. This is because as V_0 increases the ion transport is electrostatically hindered by the enriched ions inside the nanopore so that the rate of increase in J_1 with increasing V_0 is slower than the rate of increase in V_0 .²¹ However, if V_0 is sufficiently high, it becomes more significant than the electric field arising from ion enrichment so



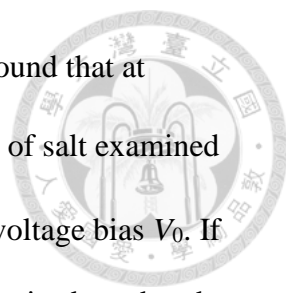
that $|J_1/V_0|$ becomes to increase with V_0 . On the other hand, since anions (co-ions) are mainly present outside the double layer, J_2 is influenced mainly by V_0 . Therefore, $|J_2/V_0|$ increases essentially with increasing V_0 , as seen in Figure 1-8(b) and (d). As seen in Figure 1-7(b), at $C_{\text{bulk}} = 100 \text{ mM}$ and $\theta = 0.5^\circ$, since the overlapping of double layer in the nanopore is insignificant, the induced electric field mentioned above is unimportant compared to that associated with V_0 . Therefore, as in Figure 1-8(a), $|J_1/V_0|$ also shows a local minimum in Figure 1-8(c), except that the latter is more apparent. Figure 1-8(a) and (c) reveals that in the latter, $|J_1/V_0|$ begins to increase with increasing V_0 at a smaller value of V_0 , and the rate of increase is much faster so that the selectivity in Figure 1-7(b) decreases non-monotonically with increasing V_0 , instead of monotonically as that in Figure 1-7(a).

1-3-6 Ion selectivity for $V_0 > 0$

The voltage-dependent selectivity when a positive voltage bias is applied is illustrated in Figure 1-S9. In this case, because the depletion of ions inside the nanopore is significant, and ion concentration low, the double layer is thick so that $S \cong 1$, and it is insensitive to the variation in V_0 , as illustrated in Figure 1-S9(a). Different from that for the case of $V_0 < 0$, Figure 1-S9(b) shows that the S for various types of salt increases with increasing V_0 . This is expected because if $V_0 > 0$, the larger the V_0 the more significant the degree of ion depletion, the more significant the overlapping of double layer, and therefore, the larger the S .

1-4. Conclusions

We investigated theoretically the ionic current rectification behavior of a negatively charged conical nanopore focusing on the influence of the half cone angle θ , the bulk

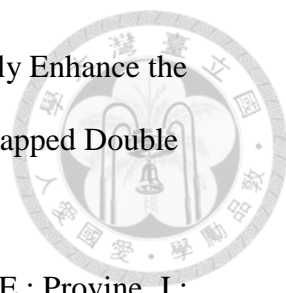



salt concentration C_{bulk} , and the type of salt (KCl, NaCl, LiCl). It is found that at $C_{\text{bulk}} = 3 \text{ mM}$ and/or $\theta < 1^\circ$, the rectification ratio R_f of the types of salt examined ranks as $R_f(\text{LiCl}) > R_f(\text{NaCl}) > R_f(\text{KCl})$ for all the levels of the applied voltage bias V_0 . If V_0 is sufficiently high, this order can be reversed if C_{bulk} and/or θ are raised, so that the $R_f - V_0$ curves of the types of salt examined intersect at the same point. This can be attributed to the difference in the degree of ion enrichment of the types of salt considered for $V_0 < 0$. The degree of enrichment of LiCl is the largest if V_0 is small regardless of the level of θ ; however, as the level of V_0 increases, the enrichment of KCl becomes the largest only if $\theta > 1^\circ$. The point of intersection of the $R_f - V_0$ curves of the types of salt examined shifts to a lower value of V_0 when either C_{bulk} or θ is increased, which can be explained by the rate of ion transport. Due to the accumulation of ions near the nanopore tip, the rate of decrease in the electric potential decreases if the overlapping of double layer is significant, thereby lowering the rate of transport of ions. However, if C_{bulk} and/or θ take a higher value, the distributions of the electric potential of the types of salt examined are essentially the same. The selectivity S for the types of salt examined ranks as $S(\text{KCl}) > S(\text{NaCl}) > S(\text{LiCl})$, and its behavior as V_0 varies depends highly on the level of C_{bulk} . If $C_{\text{bulk}} = 3 \text{ mM}$, S decreases monotonically with increasing V_0 ; if C_{bulk} is sufficiently high and θ large, S shows both a local minimum and a local maximum as V_0 varies.



References

1. Zhang, H. C.; Tian, Y.; Hou, J.; Hou, X.; Hou, G. L.; Ou, R. W.; Wang, H. T.; Jiang, L. Bioinspired Smart Gate-Location-Controllable Single Nanochannels: Experiment and Theoretical Simulation. *ACS Nano* **2015**, *9*, 12264-12273.
2. Liu, M. Y.; Zhang, H. C.; Li, K.; Heng, L. P.; Wang, S. T.; Tian, Y.; Jiang, L. A Bio-Inspired Potassium and pH Responsive Double-Gated Nanochannel. *Adv. Funct. Mater.* **2015**, *25*, 421-426.
3. Gao, L. J.; Li, P.; Zhang, Y. Q.; Xiao, K.; Ma, J.; Xie, G. H.; Hou, G. L.; Zhang, Z.; Wen, L. P.; Jiang, L. A Bio-Inspired, Sensitive, and Selective Ionic Gate Driven by Silver (I) Ions. *Small* **2015**, *11*, 543-547.
4. Xie, G. H.; Wen, L. P.; Jiang, L. Biomimetic Smart Nanochannels for Power Harvesting. *Nano Res.* **2016**, *9*, 59-71.
5. Tseng, S.; Li, Y. M.; Lin, C. Y.; Hsu, J. P. Salinity Gradient Power: Influences of Temperature and Nanopore Size. *Nanoscale* **2016**, *8*, 2350-2357.
6. Zhang, Z.; Kong, X. Y.; Xiao, K.; Liu, Q.; Xie, G. H.; Li, P.; Ma, J.; Tian, Y.; Wen, L. P.; Jiang, L. Engineered Asymmetric Heterogeneous Membrane: A Concentration-Gradient-Driven Energy Harvesting Device. *J. Am. Chem. Soc.* **2015**, *137*, 14765-14772.
7. Cao, L. X.; Guo, W.; Ma, W.; Wang, L.; Xia, F.; Wang, S. T.; Wang, Y. G.; Jiang, L.; Zhu, D. B. Towards Understanding the Nanofluidic Reverse Electrodialysis System: Well Matched Charge Selectivity and Ionic Composition. *Energ Environ Sci* **2011**, *4*, 2259-2266.
8. Feng, J. D.; Graf, M.; Liu, K.; Ovchinnikov, D.; Dumcenco, D.; Heiranian, M.; Nandigana, V.; Aluru, N. R.; Kis, A.; Radenovic, A. Single-Layer Mos₂ Nanopores as Nanopower Generators. *Nature* **2016**, *536*, 197-200.

- 
9. Mei, L. J.; Yeh, L. H.; Qian, S. Z. Buffer Anions Can Enormously Enhance the Electrokinetic Energy Conversion in Nanofluidics with Highly Overlapped Double Layers. *Nano Energy* **2017**, *32*, 374-381.
10. Paik, K. H.; Liu, Y.; Tabard-Cossa, V.; Waugh, M. J.; Huber, D. E.; Provine, J.; Howe, R. T.; Dutton, R. W.; Davis, R. W. Control of DNA Capture by Nanofluidic Transistors. *ACS Nano* **2012**, *6*, 6767-6775.
11. He, Y. H.; Tsutsui, M.; Fan, C.; Taniguchi, M.; Kawai, T. Controlling DNA Translocation through Gate Modulation of Nanopore Wall Surface Charges. *ACS Nano* **2011**, *5*, 5509-5518.
12. Kowalczyk, S. W.; Wells, D. B.; Aksimentiev, A.; Dekker, C. Slowing Down DNA Translocation through a Nanopore in Lithium Chloride. *Nano Lett.* **2012**, *12*, 1038-1044.
13. Gu, L. Q.; Shim, J. W. Single Molecule Sensing by Nanopores and Nanopore Devices. *Analyst* **2010**, *135*, 441-451.
14. Howorka, S.; Siwy, Z. Nanopores and Nanochannels: From Gene Sequencing to Genome Mapping. *ACS Nano* **2016**, *10*, 9768-9771.
15. Ying, Y. L.; Zhang, J. J.; Gao, R.; Long, Y. T. Nanopore-Based Sequencing and Detection of Nucleic Acids. *Angew. Chem. Int. Edit.* **2013**, *52*, 13154-13161.
16. Vlassioug, I.; Kozel, T. R.; Siwy, Z. S. Biosensing with Nanofluidic Diodes. *J. Am. Chem. Soc.* **2009**, *131*, 8211-8220.
17. Ma, Y.; Su, Y. S.; Qian, S. Z.; Yeh, L. H. Analytical Model for Surface-Charge-Governed Nanochannel Conductance. *Sensor Actuat B-Chem* **2017**, *247*, 697-705.
18. Schoch, R. B.; Han, J. Y.; Renaud, P. Transport Phenomena in Nanofluidics. *RvMP* **2008**, *80*, 839-883.

- 
19. Ma, Y.; Yeh, L. H.; Lin, C. Y.; Mei, L. J.; Qian, S. Z. pH-Regulated Ionic Conductance in a Nanochannel with Overlapped Electric Double Layers. *Anal. Chem.* **2015**, *87*, 4508-4514.
20. Zangle, T. A.; Mani, A.; Santiago, J. G. Theory and Experiments of Concentration Polarization and Ion Focusing at Microchannel and Nanochannel Interfaces. *Chem. Soc. Rev.* **2010**, *39*, 1014-1035.
21. Yeh, L. H.; Zhang, M.; Qian, S.; Hsu, J. P.; Tseng, S. Ion Concentration Polarization in Polyelectrolyte-Modified Nanopores. *J. Phys. Chem. C* **2012**, *116*, 8672-8677.
22. Vlasiouk, I.; Smirnov, S.; Siwy, Z. Ionic Selectivity of Single Nanochannels. *Nano Lett.* **2008**, *8*, 1978-1985.
23. Zeng, Z. P.; Yeh, L. H.; Zhang, M. K.; Qian, S. Z. Ion Transport and Selectivity in Biomimetic Nanopores with pH-Tunable Zwitterionic Polyelectrolyte Brushes. *Nanoscale* **2015**, *7*, 17020-17029.
24. Pietschmann, J. F.; Wolfram, M. T.; Burger, M.; Trautmann, C.; Nguyen, G.; Pevarnik, M.; Bayer, V.; Siwy, Z. Rectification Properties of Conically Shaped Nanopores: Consequences of Miniaturization. *Phys. Chem. Chem. Phys.* **2013**, *15*, 16917-16926.
25. Liu, Q.; Wang, Y.; Guo, W.; Ji, H.; Xue, J.; Ouyang, Q. Asymmetric Properties of Ion Transport in a Charged Conical Nanopore. *Phys. Rev. E* **2007**, *75*, 051201.
26. Siwy, Z. S. Ion-Current Rectification in Nanopores and Nanotubes with Broken Symmetry. *Adv. Funct. Mater.* **2006**, *16*, 735-746.
27. White, H. S.; Bund, A. Ion Current Rectification at Nanopores in Glass Membranes. *Langmuir* **2008**, *24*, 2212-2218.
28. Nasir, S.; Ali, M.; Ramirez, P.; Gomez, V.; Oschmann, B.; Muench, F.; Tahir, M. N.;

Zentel, R.; Mafe, S.; Ensinger, W. Fabrication of Single Cylindrical Au-Coated Nanopores with Non-Homogeneous Fixed Charge Distribution Exhibiting High Current Rectifications. *ACS Appl. Mater. Inter.* **2014**, *6*, 12486-12494.



29. Tagliazucchi, M.; Rabin, Y.; Szeleifer, I. Transport Rectification in Nanopores with Outer Membranes Modified with Surface Charges and Polyelectrolytes. *ACS Nano* **2013**, *7*, 9085-9097.

30. Ali, M.; Ramirez, P.; Nguyen, H. Q.; Nasir, S.; Cervera, J.; Mafe, S.; Ensinger, W. Single Cigar-Shaped Nanopores Functionalized with Amphoteric Amino Acid Chains: Experimental and Theoretical Characterization. *ACS Nano* **2012**, *6*, 3631-3640.

31. Lin, C. Y.; Yeh, L. H.; Hsu, J. P.; Tseng, S. Regulating Current Rectification and Nanoparticle Transport through a Salt Gradient in Bipolar Nanopores. *Small* **2015**, *11*, 4594-4602.

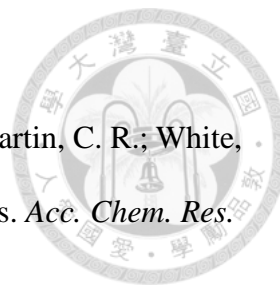
32. Zhang, Z.; Kong, X. Y.; Xiao, K.; Xie, G. H.; Liu, Q.; Tian, Y.; Zhang, H. C.; Ma, J.; Wen, L. P.; Jiang, L. A Bioinspired Multifunctional Heterogeneous Membrane with Ultrahigh Ionic Rectification and Highly Efficient Selective Ionic Gating. *Adv. Mater.* **2016**, *28*, 144-150.

33. Han, K. Y.; Heng, L. P.; Wen, L. P.; Jiang, L. Biomimetic Heterogeneous Multiple Ion Channels: A Honeycomb Structure Composite Film Generated by Breath Figures. *Nanoscale* **2016**, *8*, 12318-12323.

34. Yang, C.; Hinkle, P.; Menestrina, J.; Vlasiouk, I. V.; Siwy, Z. S. Polarization of Gold in Nanopores Leads to Ion Current Rectification. *J. Phys. Chem. Lett.* **2016**, *7*, 4152-4158.

35. Sa, N. Y.; Lan, W. J.; Shi, W. Q.; Baker, L. A. Rectification of Ion Current in Nanopipettes by External Substrates. *ACS Nano* **2013**, *7*, 11272-11282.

36. Peng, R.; Li, D. Q. Electroosmotic Flow in Single Pdms Nanochannels. *Nanoscale*



2016, 8, 12237-12246.

37. Lan, W. J.; Edwards, M. A.; Luo, L.; Perera, R. T.; Wu, X. J.; Martin, C. R.; White, H. S. Voltage-Rectified Current and Fluid Flow in Conical Nanopores. *Acc. Chem. Res.*

2016, 49, 2605-2613.

38. Ai, Y.; Zhang, M. K.; Joo, S. W.; Cheney, M. A.; Qian, S. Z. Effects of Electroosmotic Flow on Ionic Current Rectification in Conical Nanopores. *J. Phys. Chem. C* **2010**, 114, 3883-3890.

39. Lin, D. H.; Lin, C. Y.; Tseng, S.; Hsu, J. P. Influence of Electroosmotic Flow on the Ionic Current Rectification in a pH-Regulated, Conical Nanopore. *Nanoscale* **2015**, 7, 14023-14031.

40. Hsu, J. P.; Wu, H. H.; Lin, C. Y.; Tseng, S. Importance of Polyelectrolyte Modification for Rectifying the Ionic Current in Conically Shaped Nanochannels. *Phys. Chem. Chem. Phys.* **2017**, 19, 5351-5360.

41. Plett, T. S.; Cai, W. J.; Le Thai, M.; Vlassioux, I. V.; Penner, R. M.; Siwy, Z. S. Solid-State Ionic Diodes Demonstrated in Conical Nanopores. *J. Phys. Chem. C* **2017**, 121, 6170-6176.

42. Tseng, S. J.; Yang, S. T.; Lin, C. Y.; Hsu, J. P. Ionic Current Rectification in a Conical Nanopore: Influences of Electroosmotic Flow and Type of Salt. *J. Phys. Chem. C* **2017**.

43. Gamble, T.; Decker, K.; Plett, T. S.; Pevarnik, M.; Pietschmann, J. F.; Vlassioux, I.; Aksimentiev, A.; Siwy, Z. S. Rectification of Ion Current in Nanopores Depends on the Type of Monovalent Cations: Experiments and Modeling. *J. Phys. Chem. C* **2014**, 118, 9809-9819.

44. Perez-Mitta, G.; Albesa, A. G.; Molaes, M. E. T.; Trautmann, C.; Azzaroni, O. The Influence of Divalent Anions on the Rectification Properties of Nanofluidic Diodes:

Insights from Experiments and Theoretical Simulations. *Chemphyschem* **2016**, *17*, 2718-2725.

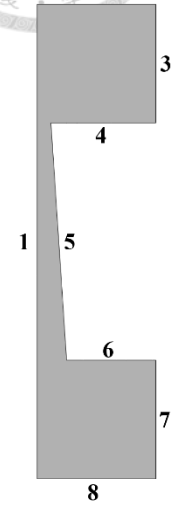
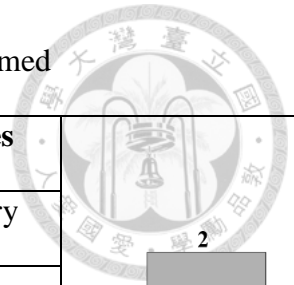
45. Lin, J.-Y.; Lin, C.-Y.; Hsu, J.-P.; Tseng, S. Ionic Current Rectification in a pH-Tunable Polyelectrolyte Brushes Functionalized Conical Nanopore: Effect of Salt Gradient. *Anal. Chem.* **2016**, *88*, 1176-1187.
46. Cao, L. X.; Guo, W.; Wang, Y. G.; Jiang, L. Concentration-Gradient-Dependent Ion Current Rectification in Charged Conical Nanopores. *Langmuir* **2012**, *28*, 2194-2199.
47. Kubeil, C.; Bund, A. The Role of Nanopore Geometry for the Rectification of Ionic Currents. *J. Phys. Chem. C* **2011**, *115*, 7866-7873.
48. Ramirez, P.; Apel, P. Y.; Cervera, J.; Mafe, S. Pore Structure and Function of Synthetic Nanopores with Fixed Charges: Tip Shape and Rectification Properties. *Nanotechnology* **2008**, *19*, 315707.
49. Tseng, S. J.; Lin, S. C.; Lin, C. Y.; Hsu, J. P. Influences of Cone Angle and Surface Charge Density on the Ion Current Rectification Behavior of a Conical Nanopore. *J. Phys. Chem. C* **2016**, *120*, 25620-25627.
50. Hsu, J. P.; Wu, H. H.; Lin, C. Y.; Tseng, S. Ion Current Rectification Behavior of Bioinspired Nanopores Having a pH-Tunable Zwitterionic Surface. *Anal. Chem.* **2017**, *89*, 3952-3958.
51. Bhattacharya, S.; Muzard, J.; Payet, L.; Mathe, J.; Bockelmann, U.; Aksimentiev, A.; Viasnoff, V. Rectification of the Current in Alpha-Hemolysin Pore Depends on the Cation Type: The Alkali Series Probed by Molecular Dynamics Simulations and Experiments. *J. Phys. Chem. C* **2011**, *115*, 4255-4264.
52. Lin, C. Y.; Chen, F.; Yeh, L. H.; Hsu, J. P. Salt Gradient Driven Ion Transport in Solid-State Nanopores: The Crucial Role of Reservoir Geometry and Size. *Phys. Chem. Chem. Phys.* **2016**, *18*, 30160-30165.

53. Steinbock, L. J.; Lucas, A.; Otto, O.; Keyser, U. F. Voltage-Driven Transport of Ions and DNA through Nanocapillaries. *Electrophoresis* **2012**, *33*, 3480-3487.



Table 1-1. Summary of the boundary conditions assumed

surface	Poisson	Nernst-Planck	Navier-Stokes
1	axial symmetry	axial symmetry	axial symmetry
2	grounded $\phi = 0$	bulk concentration $c_i = C_{\text{bulk}}$	no external pressure gradient $p = 0$
8	applied voltage $\phi = V_0$		
3, 7	charge free $-\mathbf{n} \cdot \nabla \phi = 0$	zero normal flux $\mathbf{n} \cdot \mathbf{N}_i = 0$	slip
4,5,6	surface charge density specified $-\varepsilon_f \mathbf{n} \cdot \nabla \phi = \sigma_s$	ion-impenetrable $\mathbf{n} \cdot \mathbf{N}_i = 0$	nonslip $\mathbf{u} = \mathbf{0}$



(not in scale)

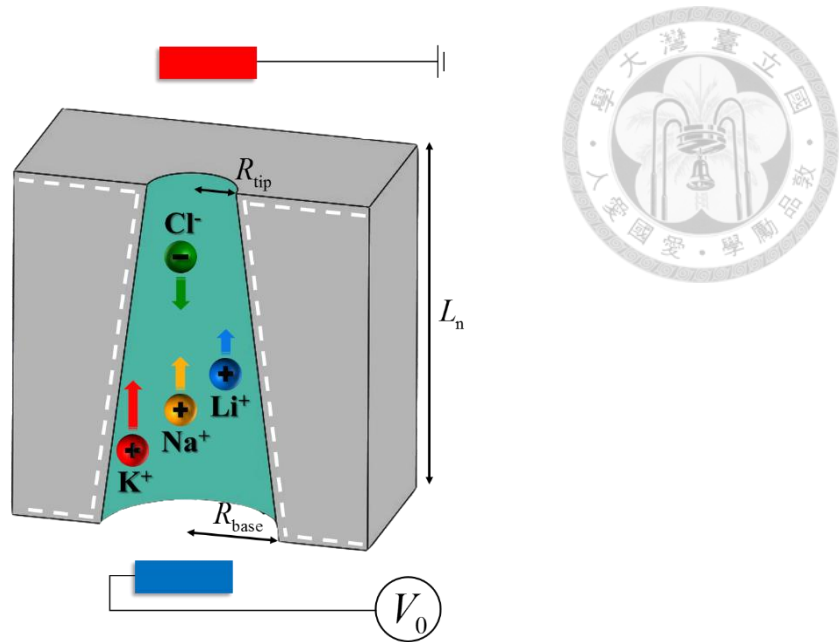


Figure 1-1. Schematic representation of the ion transport through a charged conical nanopore of tip radius R_{tip} , base radius R_{base} , and length L_n connecting two large, identical reservoirs filled with an aqueous salt solution. V_0 is the voltage bias applied across the nanopore with the electrode in the upper reservoir grounded.

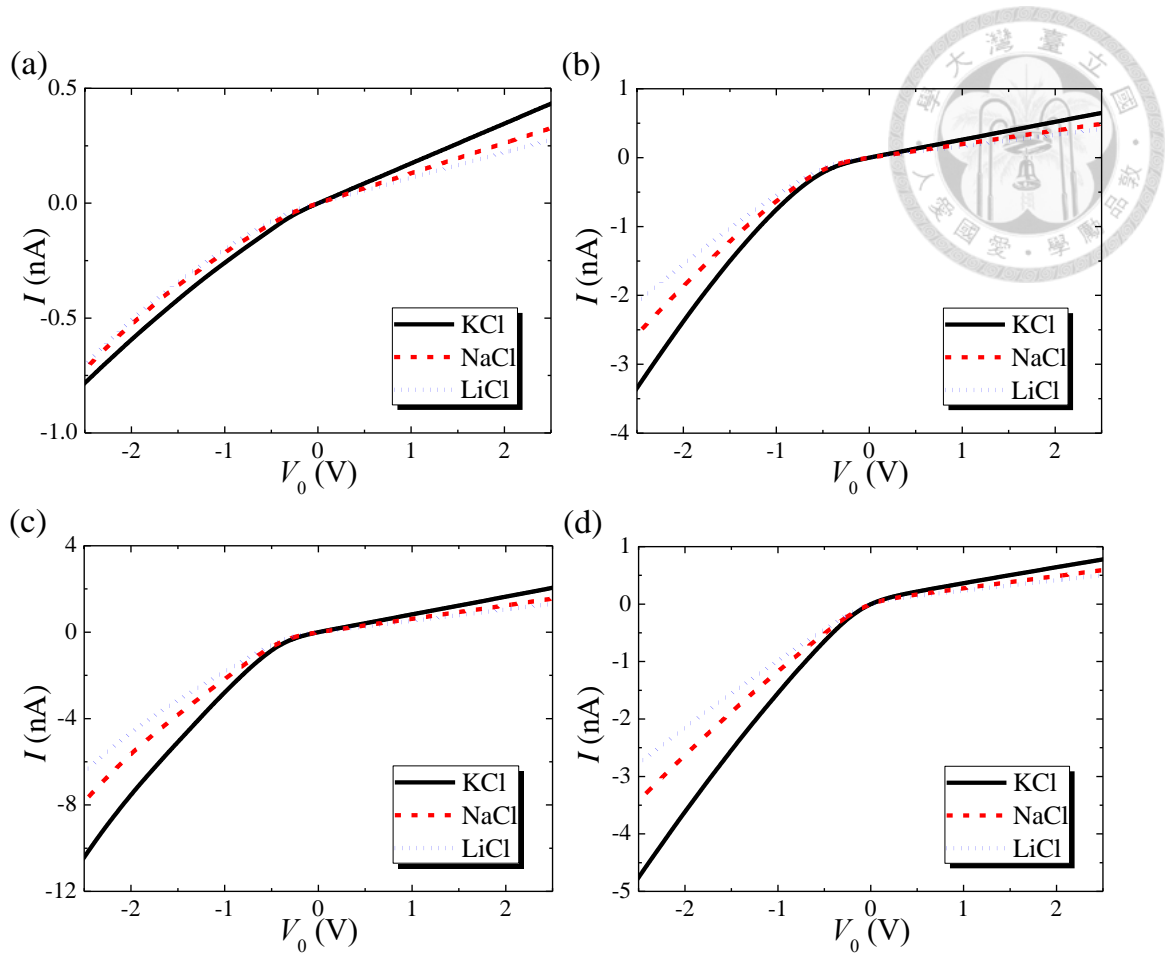


Figure 1-2. Current-voltage curves for various salt solutions at various combinations of bulk salt concentration C_{bulk} and half cone angle θ at $R_{\text{tip}} = 6 \text{ nm}$. (a) $C_{\text{bulk}} = 3 \text{ mM}$ and $\theta = 0.5^\circ$; (b) $C_{\text{bulk}} = 3 \text{ mM}$ and $\theta = 1^\circ$; (c) $C_{\text{bulk}} = 3 \text{ mM}$ and $\theta = 5^\circ$; (d) $C_{\text{bulk}} = 100 \text{ mM}$ and $\theta = 1^\circ$.

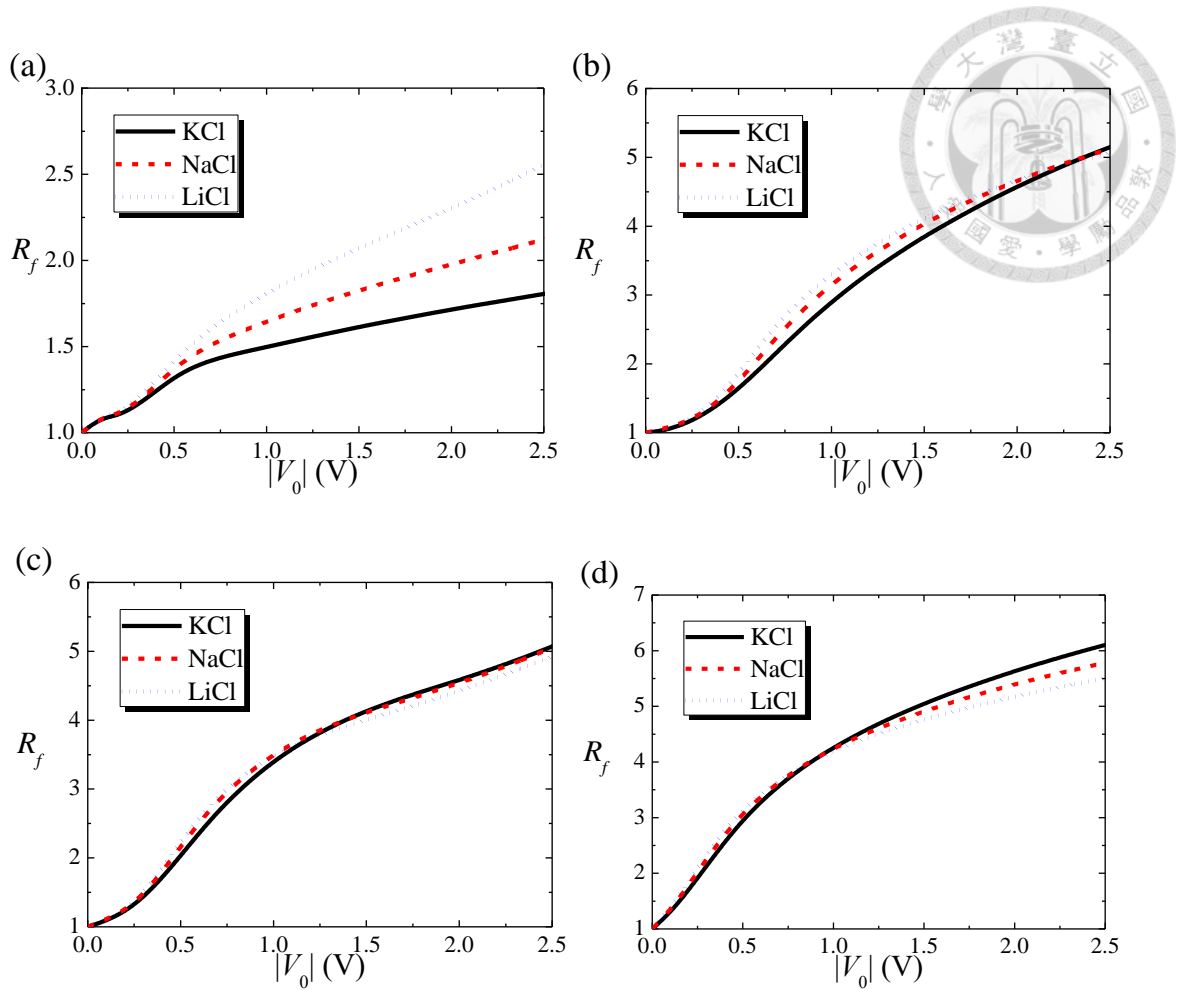


Figure 1-3. Current rectification ratio, R_f , as a function of the magnitude of the applied voltage, $|V_0|$, for various salt solutions at various combinations of the bulk salt concentration C_{bulk} and the half cone angle θ at $R_{\text{tip}} = 6 \text{ nm}$. (a) $C_{\text{bulk}} = 3 \text{ mM}$ and $\theta = 0.5^\circ$; (b) $C_{\text{bulk}} = 3 \text{ mM}$ and $\theta = 1^\circ$; (c) $C_{\text{bulk}} = 3 \text{ mM}$ and $\theta = 5^\circ$; (d) $C_{\text{bulk}} = 100 \text{ mM}$ and $\theta = 1^\circ$.

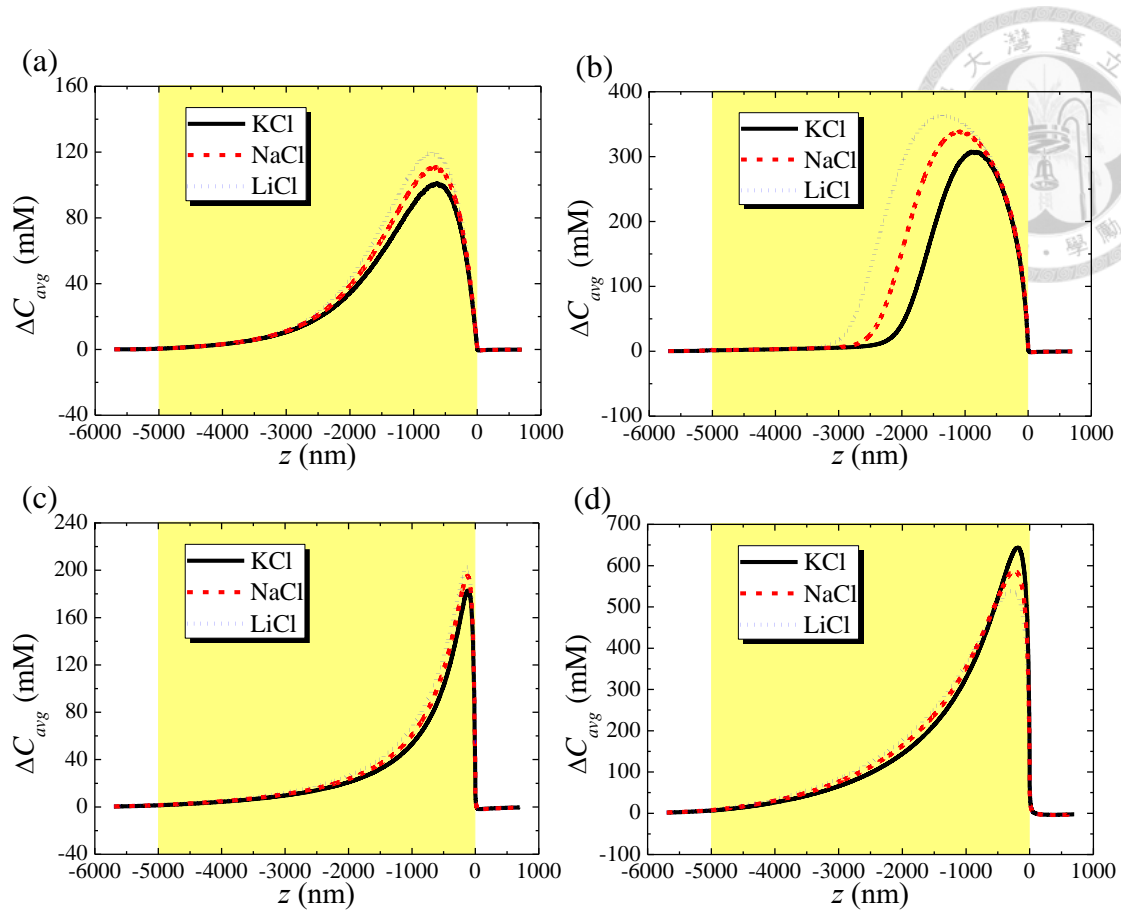


Figure 1-4. Axial variations in the cross sectional averaged concentration difference ΔC_{avg} at $C_{bulk} = 3$ mM and $R_{tip} = 6$ nm for various combinations of the half cone angle θ and the applied voltage bias V_0 . (a) $\theta = 0.5^\circ$ and $V_0 = -0.5$ V (b) $\theta = 0.5^\circ$ and $V_0 = -1.5$ V, (c) $\theta = 5^\circ$ and $V_0 = -0.5$ V, (d) $\theta = 5^\circ$ and $V_0 = -1.5$ V.

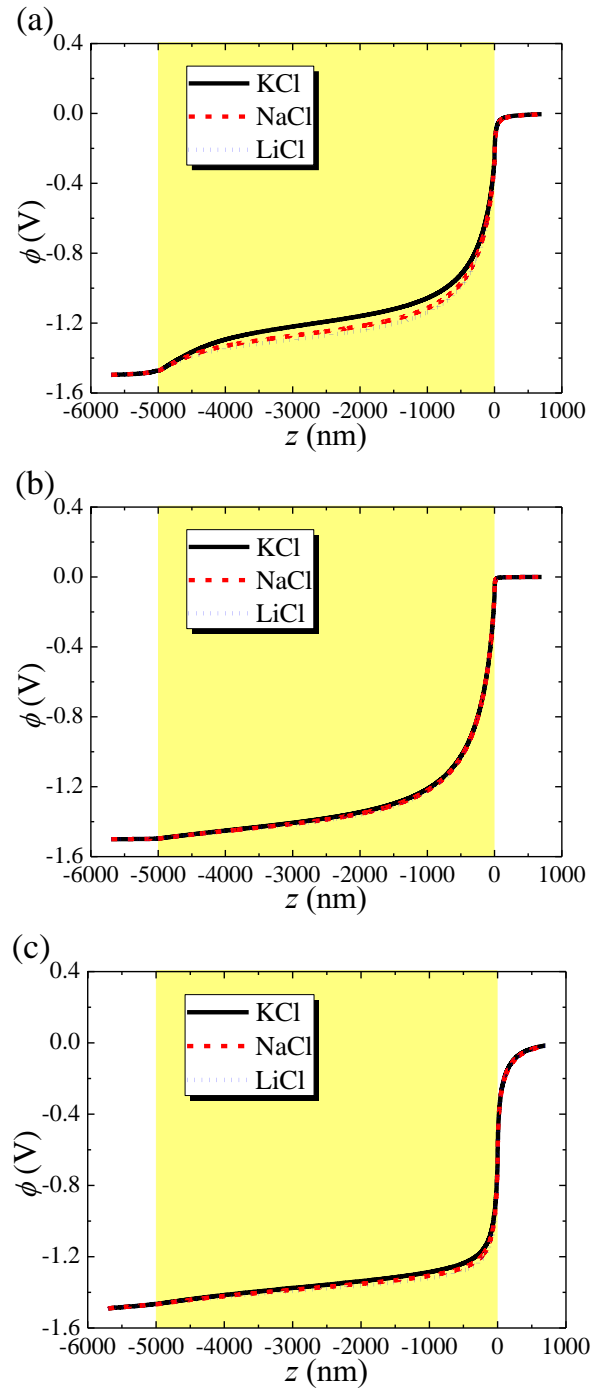


Figure 1-5. Axial variation of the cross sectional averaged electric potential at $V_0 = -1.5$ V and $R_{\text{tip}} = 6$ nm under various conditions. (a) $C_{\text{bulk}} = 3$ mM and $\theta = 1^\circ$; (b) $C_{\text{bulk}} = 100$ mM and $\theta = 1^\circ$; (c) $C_{\text{bulk}} = 3$ mM and $\theta = 5^\circ$.

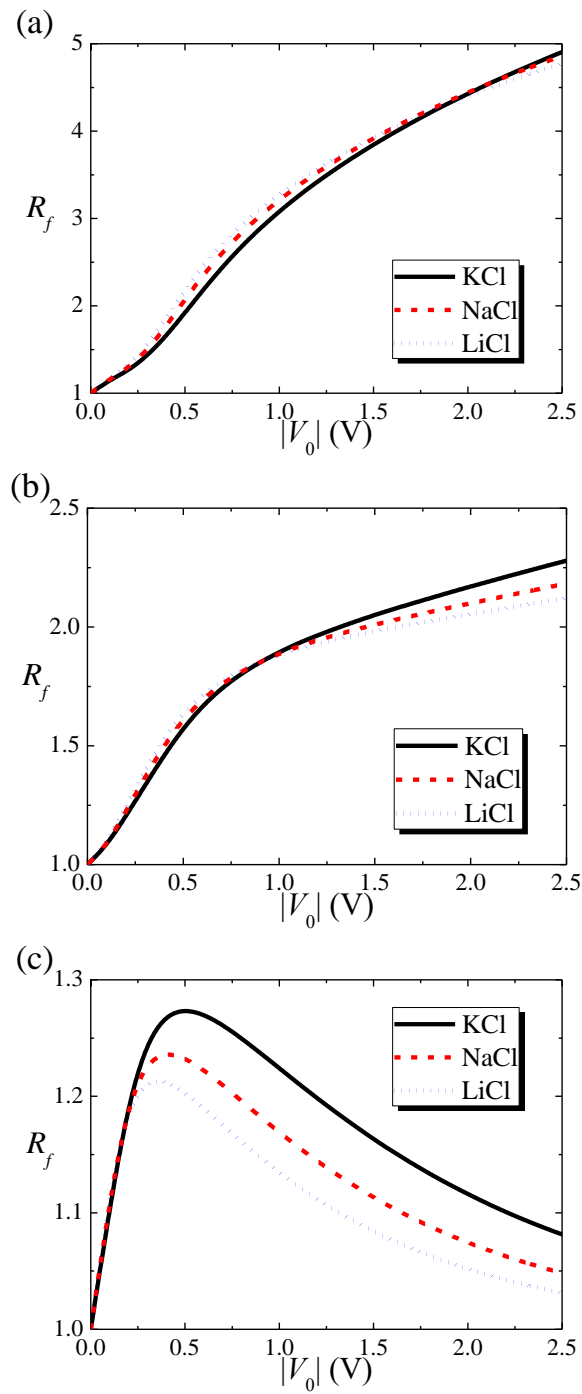


Figure 1-6. Variation of the current rectification ratio R_f with the magnitude of the applied voltage $|V_0|$ for various salts. (a): $R_{tip} = 6$ nm, $C_{bulk} = 10$ mM, and $\theta = 0.5^\circ$; (b): $R_{tip} = 15$ nm, $C_{bulk} = 10$ mM, and $\theta = 0.5^\circ$; (c): $R_{tip} = 30$ nm, $C_{bulk} = 100$ mM, and $\theta = 5^\circ$.

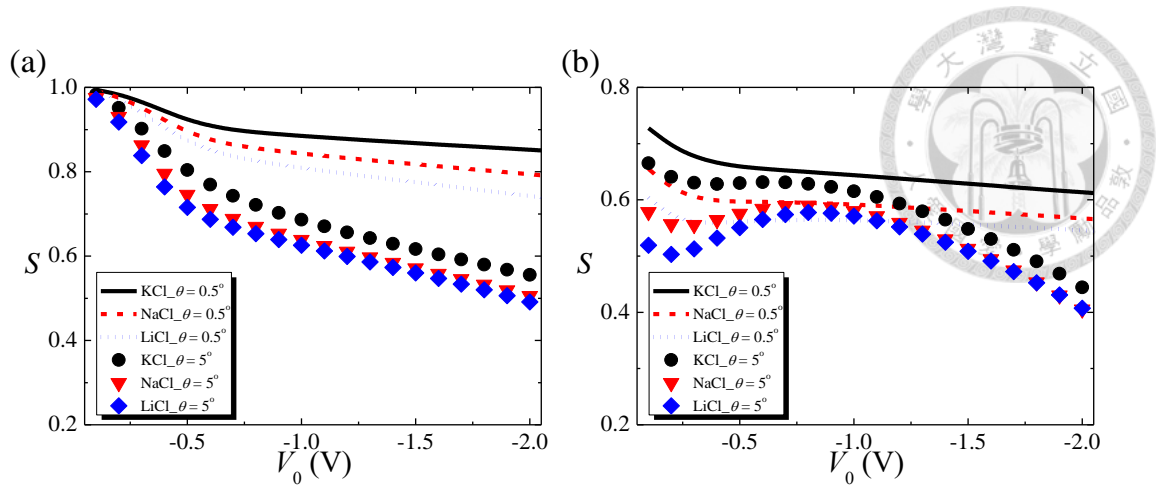


Figure 1-7. Variation of the ion selectivity S with the applied voltage bias V_0 at $R_{\text{tip}} = 6 \text{ nm}$ for various combinations of the type of salt and the half cone angle θ at $C_{\text{bulk}} = 3 \text{ mM}$, (a), and $C_{\text{bulk}} = 100 \text{ mM}$, (b).

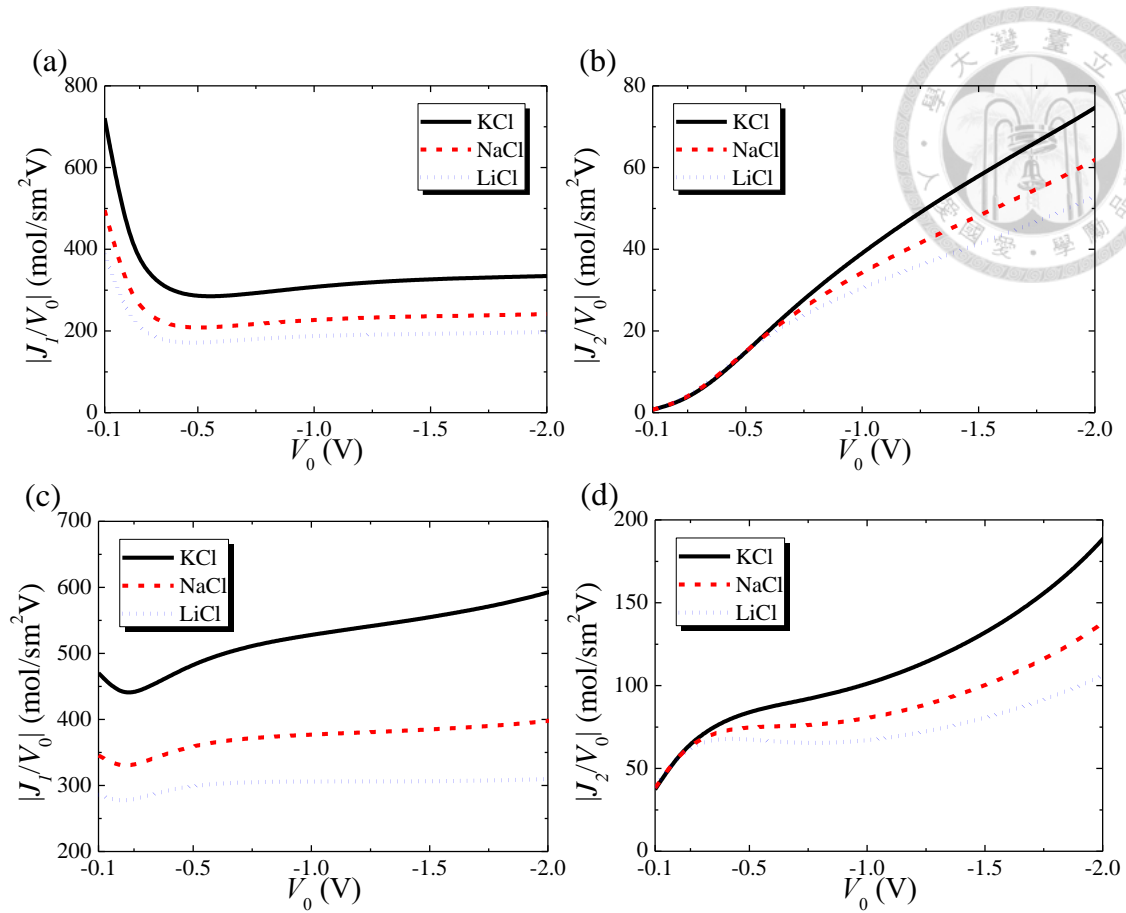


Figure 1-8. Variation of $|J_i/V_0|$ with V_0 for two levels of C_{bulk} , where J_1 (J_2) is the cross sectional averaged flux of cations (anions) at $z=0$ for $\theta = 5^\circ$ and $R_{\text{tip}} = 6 \text{ nm}$. (a) and (b): $C_{\text{bulk}} = 3 \text{ mM}$; (c) and (d): $C_{\text{bulk}} = 100 \text{ mM}$.

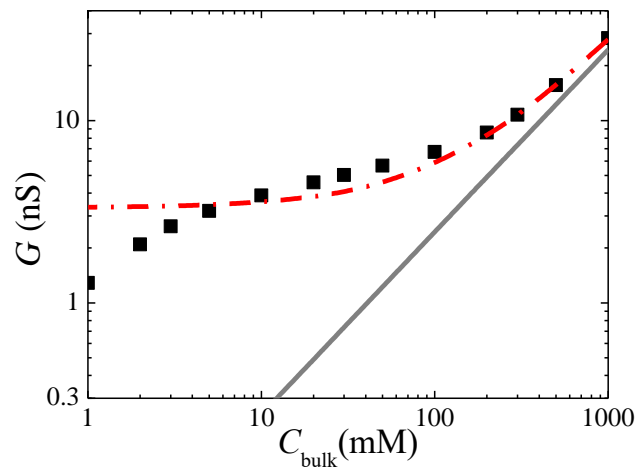


Figure 1-S1. Variation of the conductance G with the bulk salt concentration C_{bulk} .

Solid curve: bulk solution conductance; broken curve: analytic result at a constant surface charge density;⁵³ discrete symbols: present numerical result at $R_{\text{tip}}=6$ nm, $R_{\text{base}}=93.49$ nm, and $\sigma_s = -0.5$ e/nm².

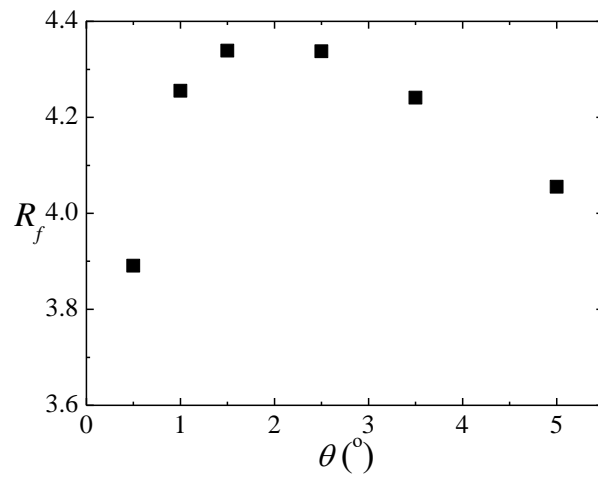


Figure 1-S2. Current rectification ratio R_f as a function of the half cone angle θ for an aqueous KCl solution at $R_{\text{tip}} = 6 \text{ nm}$ and $C_{\text{bulk}} = 100 \text{ mM}$.

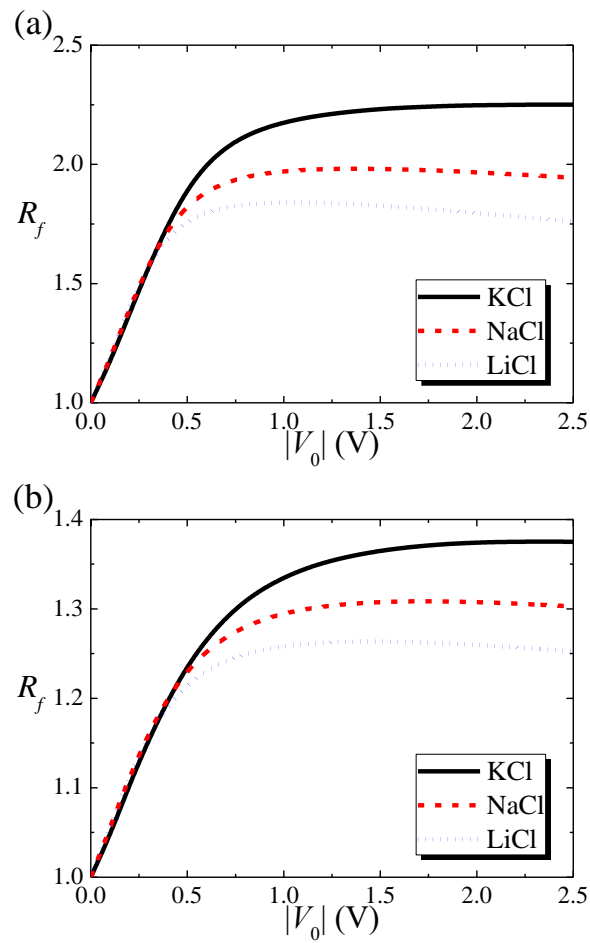


Figure 1-S3. Current rectification ratio, R_f , as a function of the magnitude of the applied voltage, $|V_0|$, for various salt solutions at $R_{\text{tip}} = 6$ nm and $\theta = 1^\circ$. (a) $C_{\text{bulk}} = 300$ mM; (b) $C_{\text{bulk}} = 1000$ mM.

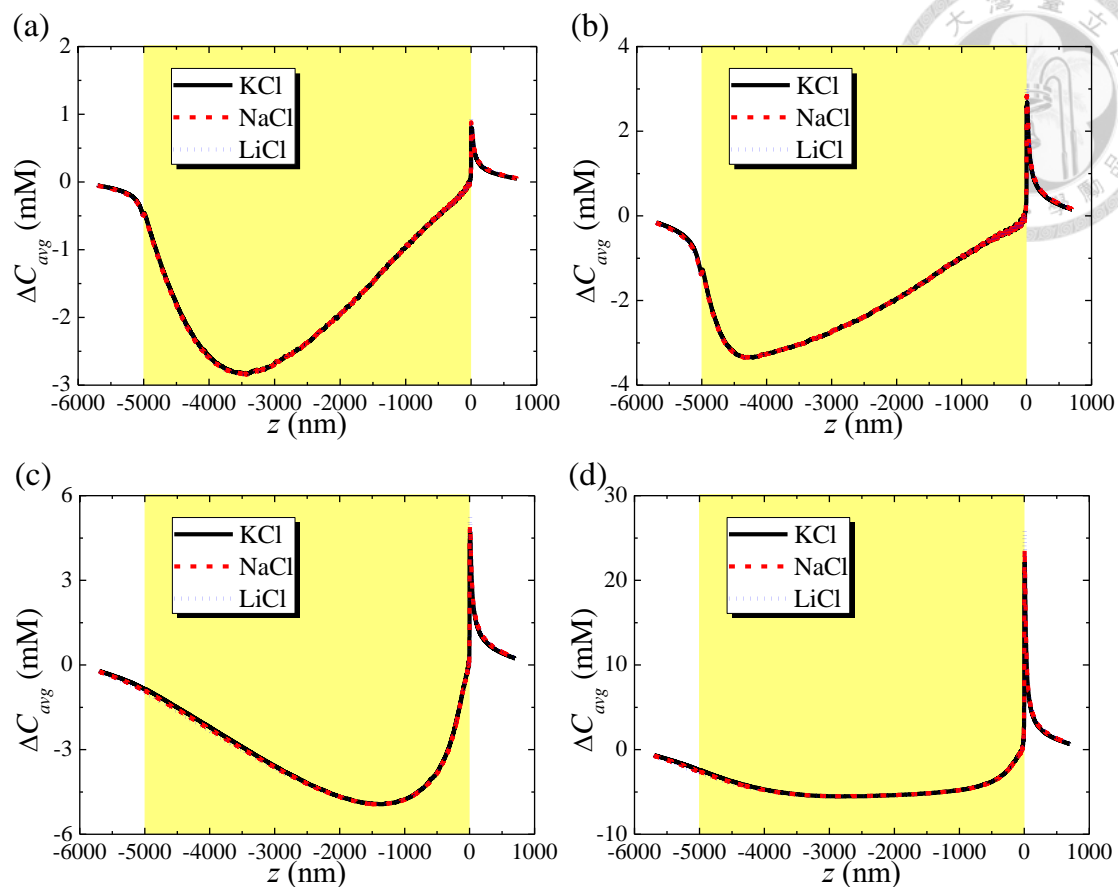


Figure 1-S4. Axial variations in the cross sectional averaged concentration difference ΔC_{avg} under various conditions, where $R_{tip} = 6$ nm . (a) $C_{bulk} = 3$ mM, $\theta = 0.5^\circ$, and $V_0 = +0.5$ V (b) $C_{bulk} = 3$ mM, $\theta = 0.5^\circ$, and $V_0 = +1.5$ V, (c) $C_{bulk} = 3$ mM, $\theta = 5^\circ$, and $V_0 = +0.5$ V, (d) $C_{bulk} = 3$ mM, $\theta = 5^\circ$, and $V_0 = +1.5$ V .

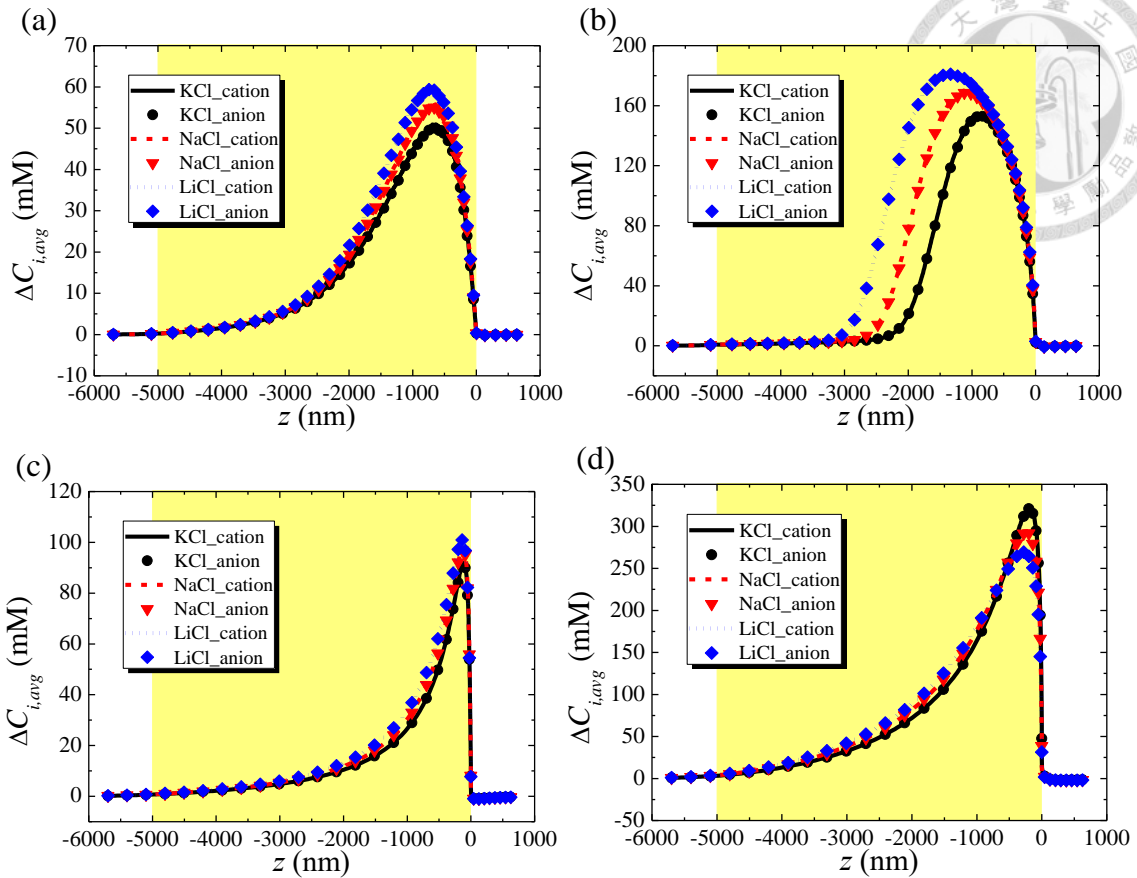


Figure 1-S5. Axial variations in the cross sectional averaged concentration difference $\Delta C_{i,avg}$ under various conditions, where $R_{tip} = 6 \text{ nm}$. (a) $C_{bulk} = 3 \text{ mM}$, $\theta = 0.5^\circ$ and $V_0 = -0.5 \text{ V}$ (b) $C_{bulk} = 3 \text{ mM}$, $\theta = 0.5^\circ$, and $V_0 = -1.5 \text{ V}$, (c) $C_{bulk} = 3 \text{ mM}$, $\theta = 5^\circ$, and $V_0 = -0.5 \text{ V}$, (d) $C_{bulk} = 3 \text{ mM}$, $\theta = 5^\circ$, and $V_0 = -1.5 \text{ V}$. Curves: cations; discrete symbols: anions.

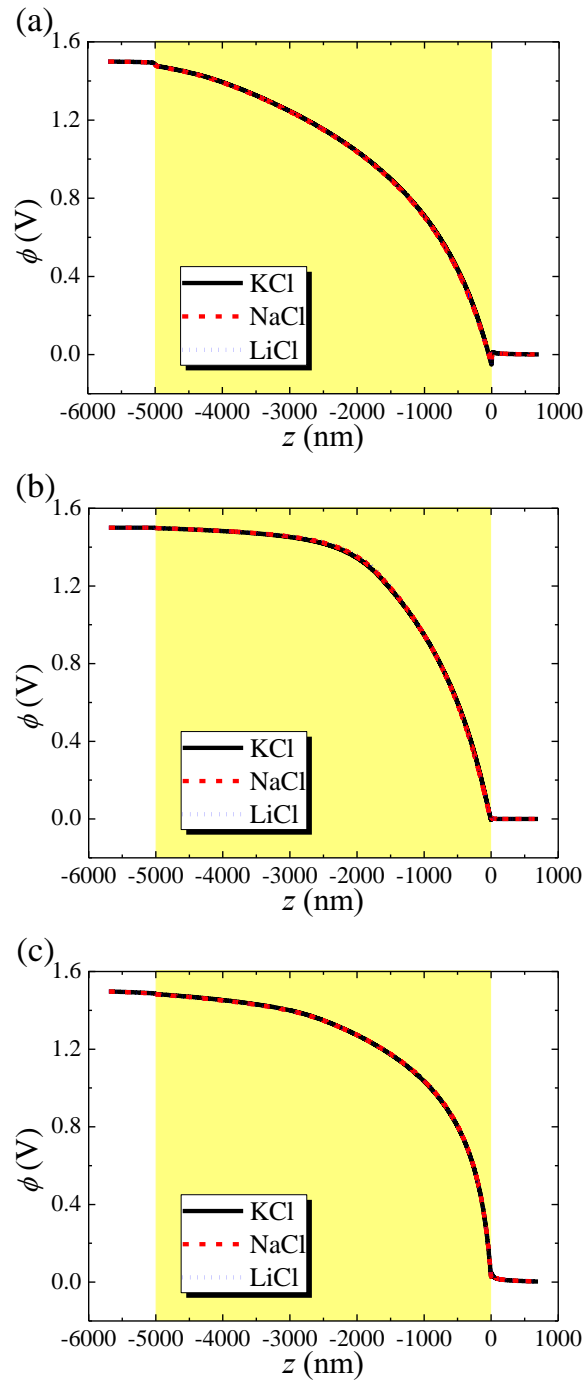


Figure 1-S6. Axial variations of the electric potential ϕ at $V_0 = +1.5$ V under various conditions, where $R_{\text{tip}} = 6$ nm (a) $C_{\text{bulk}} = 3$ mM and $\theta = 1^\circ$; (b) $C_{\text{bulk}} = 100$ mM and $\theta = 1^\circ$; (c) $C_{\text{bulk}} = 3$ mM and $\theta = 5^\circ$.

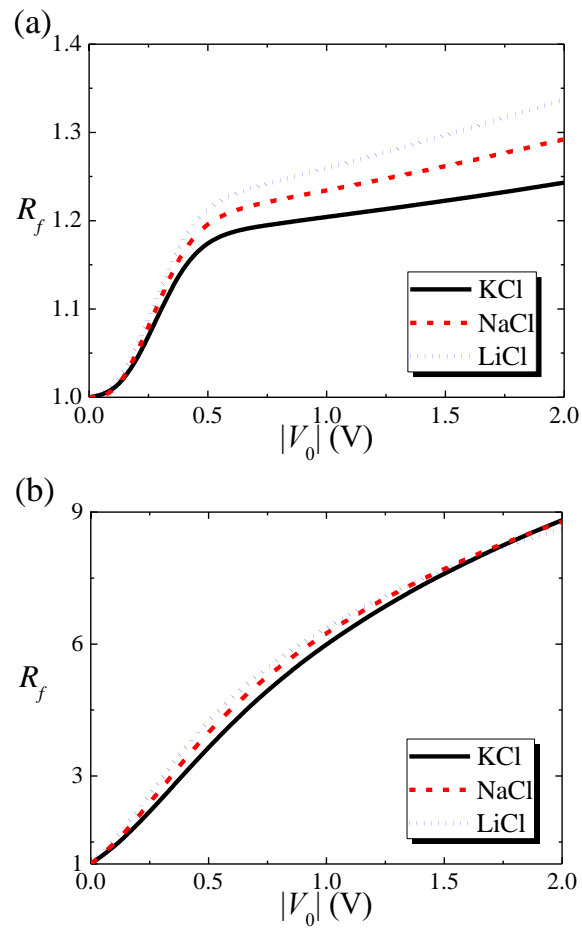


Figure 1-S7. Current rectification ratio, R_f , as a function of the magnitude of the applied voltage, $|V_0|$, for various salt solutions at $R_{\text{tip}} = 3 \text{ nm}$. (a) $C_{\text{bulk}} = 3 \text{ mM}$ and $\theta = 0.5^\circ$; (b) $C_{\text{bulk}} = 100 \text{ mM}$ and $\theta = 1^\circ$.

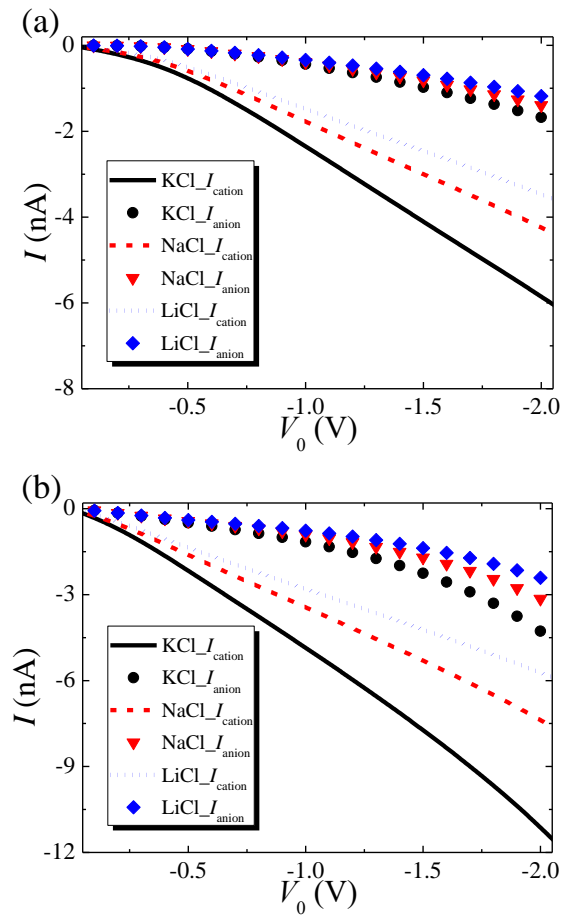


Figure 1-S8. Ionic current-voltage curves for various electrolyte solutions at various combination of salt concentration C_{bulk} and half cone angle θ , where $R_{\text{tip}} = 6 \text{ nm}$. (a) $C_{\text{bulk}} = 3 \text{ mM}$ and $\theta = 5^\circ$; (b) $C_{\text{bulk}} = 100 \text{ mM}$ and $\theta = 5^\circ$.

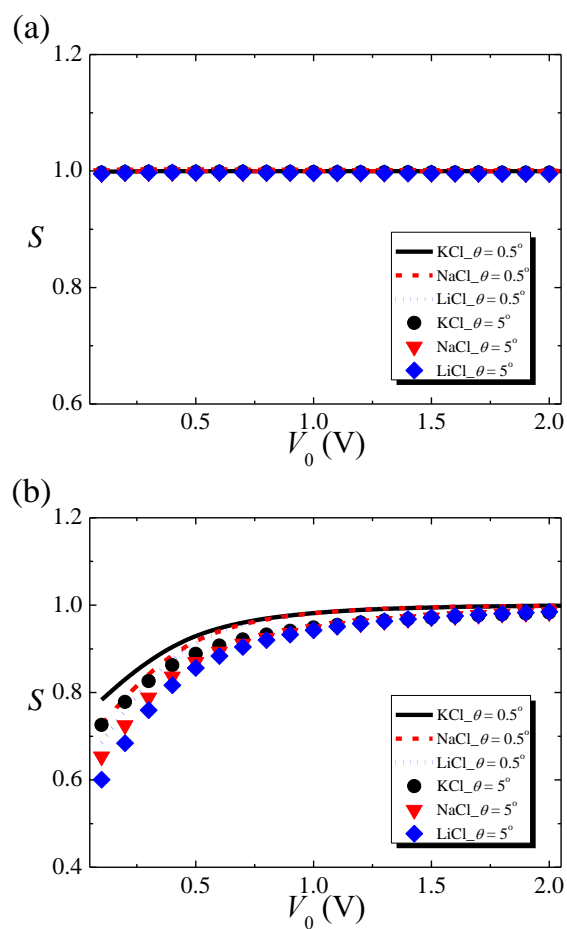
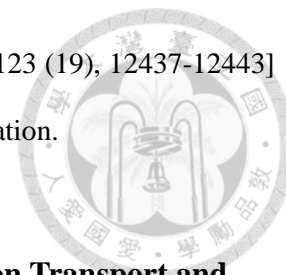
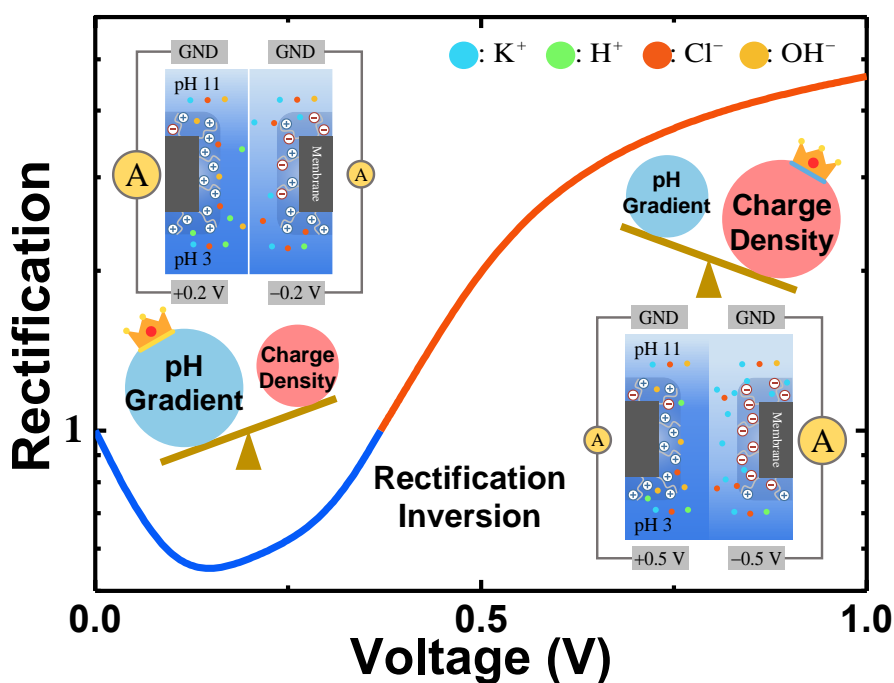
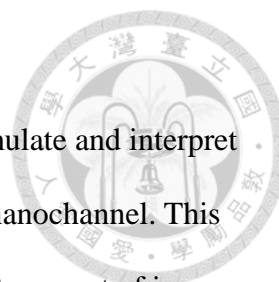


Figure 1-S9. Variation of the selectivity S with the applied voltage bias V_0 when $R_{\text{tip}} = 6 \text{ nm}$ for various combinations of the type of salt and the half cone angle θ at $C_{\text{bulk}} = 3 \text{ mM}$, (a), and $C_{\text{bulk}} = 100 \text{ mM}$, (b).



Chapter 2 Dual pH-Gradient and Voltage Modulation of Ion Transport and Current Rectification in Biomimetic Nanopores Functionalized with pH-Tunable Polyelectrolyte



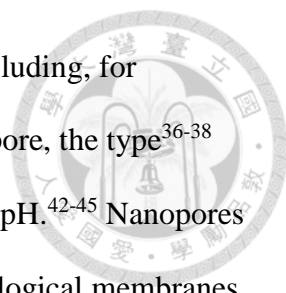


2-1. Introduction

Modern advanced fabrication techniques make it possible to simulate and interpret the behaviors of biological ion channels through artificial nanopore/nanochannel. This type of nanopore/nanochannel is also widely adopted to regulate the transport of ions, thereby facilitating potential applications in areas such as ion pumps,¹⁻³ energy conversion,⁴⁻⁸ ion gates,⁹⁻¹¹ metal ion sensing,¹²⁻¹⁴ and bio-sensors.¹⁵⁻¹⁷ To realize these applications, a thorough understanding of the phenomena and the underlying mechanisms associated with the ion transport in a micro-/nano-scaled space, which are not present in larger scaled systems, is necessary and inevitable. These phenomena include, for example, ion selectivity¹⁸⁻¹⁹ and ion current rectification (ICR).²⁰⁻²² Due to the dissociation of its functional groups, membrane surface is usually charged in an aqueous solution, making it ion-selective. Featuring in a preferential ionic current direction, ICR arises mainly from an asymmetric ion distribution inside a nanopore/nanochannel when a potential bias is applied across its two ends.

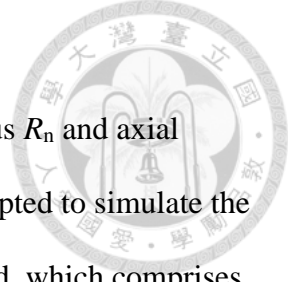
Among the synthetic nanopores proposed, biomimetic nanopores surface modified by polyelectrolytes (PE)²³⁻²⁵ gain much attention, recently. Zhang et al.,²⁶ for example, concluded that a conical polyethylene terephthalate (PET) nanopore with its tip and base sides coated with different types of polyethylene membrane having different densities exhibits a better gating behavior than the corresponding naked PET membrane. Compared with that of the corresponding solid-state nanopores, the ICR ability of nanopores surface modified with PE brushes can be several times higher.²⁷⁻²⁹ This is because the latter can attract more amount of counterions, leading to a more significant overlapping of electric double layer (EDL).³⁰⁻³¹

The transport of ions in a PE-modified nanopore was studied extensively in the last decade; both theoretical and experimental results are ample in the literature. It was



reported that the associated behavior can be influenced by factors including, for example, the geometry³²⁻³³ and the charged conditions³⁴⁻³⁵ of a nanopore, the type³⁶⁻³⁸ and the concentration³⁹⁻⁴¹ of salt in the liquid phase, and the solution pH.⁴²⁻⁴⁵ Nanopores surface modified with pH-tunable PE are often adopted to mimic biological membranes. Ali et al.⁴⁶ concluded that the charged conditions of the carboxyl groups and lysine chains on the openings of a cigar-shaped nanopore, and therefore, its ICR behavior, can be regulated by solution pH. Zeng et al.⁴⁷ reported that the ion selectivity of a PE brushes grafted cylindrical nanopore is also affected by this factor. The influence of solution pH on the ionic transport in a nanopore was studied theoretically by many investigators. However, most of them assumed a uniform pH profile across a nanopore. Several experimental studies considered a non-uniform pH profile through applying an extra pH gradient across a nanopore.^{26, 48-50} Unfortunately, there is a lack of both a comprehensive theoretical study and a detailed understanding of the underlying mechanisms. Wang et al.⁵¹ illustrated that the ICR performance of a PET conical nanopore can be enhanced by applying an additional pH gradient, implying that it can improve the efficiency of the associated electrokinetic phenomenon.

To examine thoroughly the electrokinetic transport behavior in a nanopore under various conditions and investigate comprehensively the underlying mechanisms when both an electrical potential gradient and a pH gradient are applied simultaneously, we consider a cylindrical nanopore surface functionalized with a homogeneous (single) pH-tunable PE layer. For completeness, the effect of electroosmotic flow (EOF) is also taken into account.⁵²⁻⁵⁴ The strength of the applied pH and electrical potential gradients, and the grafting density of the PE chains are examined for their influences on the conductance of the nanopore and its ICR performance.



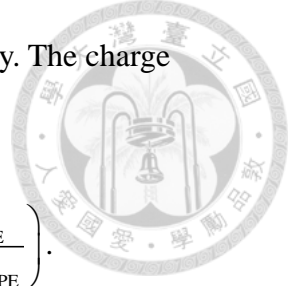
2-2. Theoretical Model

As illustrated in Figure 2-1(a), a cylindrical nanopore of radius R_n and axial length L_n connecting two large, identical cylindrical reservoirs is adopted to simulate the present problem. For convenience, a computational domain is defined, which comprises a large cylindrical region in each reservoir and the nanopore. The length and the radius of the computational domain in each reservoir are verified to be sufficiently large to ensure that the salt concentration on its boundaries reaches essentially the bulk value. The nanopore surface is modified with PE brushes layer having the thickness R_s . The geometry of the system under consideration suggests using the azimuthally symmetric cylindrical coordinates (r, z) with r and z being the radial and the axial distances, respectively. The origin is placed at the center of the nanopore interior. The system considered is filled with an aqueous salt solution containing N types of ionic species. In addition to a potential bias V_{applied} , a pH gradient is also applied across the nanopore with the bulk pH in the lower reservoir pH_L and that in the upper reservoir pH_H .

Suppose that the PE layer are pH-tunable, having acidic functional groups $-\text{COOH}$ and basic functional groups $-\text{HN}_2$ with dissociation reactions $\text{PE}-\text{COOH} \leftrightarrow \text{PE}-\text{COO}^- + \text{H}^+$ and $\text{PE}-\text{NH}_3^+ \leftrightarrow \text{PE}-\text{HN}_2 + \text{H}^+$, respectively, and associated equilibrium constants $K_A = \Gamma_{\text{PE-COO}^-} [\text{H}^+]_{\text{PE}} / \Gamma_{\text{PE-COOH}}$ and $K_B = \Gamma_{\text{PE-NH}_2} [\text{H}^+]_{\text{PE}} / \Gamma_{\text{PE-NH}_3^+}$.⁴⁰ $[\text{H}^+]_{\text{PE}}$ and Γ_k are the molar concentration of H^+ near the PE brushes and the volume number density of the functional groups k ($\text{PE}-\text{COOH}$, $\text{PE}-\text{COO}^-$, $\text{PE}-\text{HN}_2$, and $\text{PE}-\text{NH}_3^+$) of the PE layer, respectively.

If we let Γ_A and Γ_B be the total volume number densities of the acidic and basic functional groups, respectively, then $\Gamma_A = N_{\text{total}} / R_s = \Gamma_{\text{PE-COO}^-} + \Gamma_{\text{PE-COOH}}$ and

$\Gamma_B = N_{\text{total}} / R_s = \Gamma_{\text{PE-NH}_2} + \Gamma_{\text{PE-NH}_3^+}$. Here, N_{total} and Γ_{\bullet} denote the surface number



density of PE chains and that of the functional groups \bullet , respectively. The charge density of the PE brushes layer, ρ_m (C/m³), can be expressed as

$$\rho_m = 10^{27} e(-\Gamma_{\text{PE-COO}^-} + \Gamma_{\text{PE-NH}_3^+}) = 10^{27} e \left(-\frac{K_A \Gamma_A}{K_A + [\text{H}^+]_{\text{PE}}} + \frac{\Gamma_B [\text{H}^+]_{\text{PE}}}{K_B + [\text{H}^+]_{\text{PE}}} \right).$$

Let us consider the case where KCl is the background salt and the solution pH adjusted by HCl and KOH so that four kinds of ionic species ($N=4$) are present in the liquid phase: K^+ , Cl^- , H^+ , and OH^- . Let $[\text{H}^+]_0$, C_{i0} ($i=1-4$), and C_{bulk} be the bulk molar concentration of H^+ (M), that of ionic species j , and the background concentration of KCl, respectively. Then $\text{pH} = -\log[\text{H}^+]_0$, $C_{10} = C_{\text{bulk}}$,

$$C_{20} = C_{\text{bulk}} + 10^{-\text{pH}+3} - 10^{-(14-\text{pH})+3}, \quad C_{30} = 10^{-\text{pH}+3}, \quad \text{and} \quad C_{40} = 10^{-(14-\text{pH})+3} \quad \text{for} \quad \text{pH} \leq 7;$$

$$C_{10} = C_{\text{bulk}} - 10^{-\text{pH}+3} + 10^{-(14-\text{pH})+3}, \quad C_{20} = C_{\text{bulk}}, \quad C_{30} = 10^{-\text{pH}+3}, \quad \text{and} \quad C_{40} = 10^{-(14-\text{pH})+3} \quad \text{for} \quad \text{pH} > 7.$$

Assuming steady-state and small Reynolds number, the present problem can be described by the following set of equations:

$$\nabla^2 \phi = -\frac{\rho_e + h\rho_m}{\varepsilon_f} \quad (1)$$

$$\nabla \cdot \mathbf{J}_i = \nabla \cdot \left(\mathbf{u}C_i - D_i \nabla C_i - z_j \frac{D_i}{RT} FC_i \nabla \phi \right) = 0, \quad i=1, 2, 3, \text{ and } 4 \quad (2)$$

$$\nabla \cdot \mathbf{u} = 0 \quad (3)$$

$$-\nabla p + \mu \nabla^2 \mathbf{u} - \rho_e \nabla \phi - h\gamma_m \mathbf{u} = \mathbf{0} \quad (4)$$

In these expressions, ϕ , p , and \mathbf{u} are the electrical potential, the hydrodynamic pressure,

and the fluid velocity, respectively. $\rho_e = \sum_{i=1}^4 Fz_i C_i$ is the space charge density of

mobile ions, ε_f the fluid permittivity, F Faraday constant, R gas constant, T the

absolute temperature, and μ the fluid viscosity, respectively. The index h appears in eqs

1 and 4 takes account of the presence of the PE layer (h is 0 or 1 for the region outside or inside it), and γ_m is the hydrodynamic friction coefficient of that layer. \mathbf{J}_i , C_i , D_i , and z_i are the flux, concentration, diffusivity, and valence of the i th ionic species, respectively. For simplicity, the possible change in the morphology of the PE layer due to fluid flow is neglected.⁵⁵⁻⁵⁶

To specify the boundary conditions associated with eqs 1-4, we assume the following. (i) The rigid surface of nanopore walls (surfaces 4, 5, and 6, see table below) are ion-impenetrable ($\mathbf{n} \cdot \mathbf{J}_i = 0$), uncharged ($-\mathbf{n} \cdot \nabla \phi = 0$), and nonslip ($\mathbf{u} = \mathbf{0}$). (ii) The length and the radius of the computational domain in each reservoir are 1000 nm, its side boundaries (surfaces 3 and 7) have zero normal flux ($\mathbf{n} \cdot \mathbf{J}_i = 0$), and are free of charge ($-\mathbf{n} \cdot \nabla \phi = 0$) and slip. (iii) The end surfaces of the computational domain (surfaces 2 and 8) are sufficiently far from the nanopore, where surface 2 in the top reservoir is grounded ($\phi = 0$), and a voltage bias ($\phi = V_{\text{applied}}$) is applied to surface 8 in the bottom reservoir. (iv) The ionic concentration on surfaces 2 and 8 reaches essentially the bulk value ($C_i = C_{i0}$). (v) The electric potential, electric field, ionic concentrations, and flow field are all continuous on the PE layer/liquid interface (surface 9). These are summarized in Table 2-1.

2-3. Results and Discussions

The nonlinear, coupled equations governing the system under consideration, eqs 1-4, are solved numerically by COMSOL subject to the boundary conditions assumed. To this end, Multiphysics (version 4.3a, <http://www.comsol.com>) operated at a high-performance cluster is adopted. For illustration, we assume $R_n = 10$ nm, $L_n = 100$ nm, $R_s = 5$ nm, and $\lambda = 1$ nm (typical value for biological PE is ca. 0.1-10

nm),⁵⁷ where $\lambda = (\mu / \gamma_m)^{1/2}$ is the softness degree of the PE layer.⁵⁸ In addition, $\text{pK}_A = 2.2$ (α -carboxylic group) and $\text{pK}_B = 9$ (α -amino group) so that the isoelectric point (IEP) of the PE layer is 5.6.⁴² Typically, the grafting density of PE chains is on the order of 0.1 chains/nm². Therefore, two values are assumed for N_{total} : 0.1 and 0.5 chains/nm². Based on these parameters, we examine in detail the influences of the applied pH gradient and the electric voltage bias on the behavior of system under consideration. For illustration, pH_L is fixed at 3, and two levels are assumed for pH_H : 7 and 11.

Figure 2-1(b) and (c) shows several typical current-voltage (I - V) curves, where their nonlinear behaviors illustrate the ICR characteristic of the present nanopore. In our case, this characteristic is influenced mainly by the electric voltage bias V_{applied} , the level of (pH_H/pH_L), and the grafting density of the PE chains N_{total} . For convenience, we define the conductance G and the ICR factor R_f as

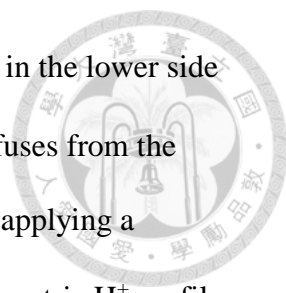
$$G = I / V_{\text{applied}} = \left[\int_S F \left(\sum_{i=1}^4 z_i \mathbf{J}_i \right) \cdot \mathbf{n} dS \right] / V_{\text{applied}} \quad (5)$$

$$R_f = \left| I(V_{\text{applied}} < 0) / I(V_{\text{applied}} > 0) \right|, \quad (6)$$

where S denotes either ends of the two reservoirs.

2-3-1 Conductance at $\text{pH}_H/\text{pH}_L=11/3$

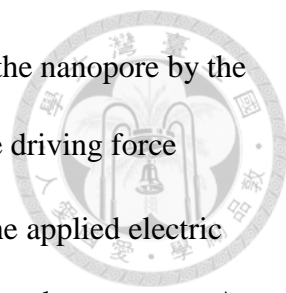
Figure 2-2(a) shows that at $\text{pH}_H/\text{pH}_L=11/3$ if $V_{\text{applied}} < 0$, the nanopore conductance G increases appreciably with increasing $|V_{\text{applied}}|$. In contrast, if $V_{\text{applied}} > 0$, G is insensitive to the variation in V_{applied} . The behavior of the nanopore conductance as the applied potential bias varies depends highly on the charge density of its PE layer, tuned



by local pH in the nanopore. Referring to Figure 2-1(a), since the pH in the lower side reservoir is lower than that in the upper side reservoir, H^+ (OH^-) diffuses from the lower (upper) side of the nanopore to its upper (lower) side. Without applying a potential bias ($V_{\text{applied}} = 0$), the applied pH gradient results in an asymmetric H^+ profile inside the nanopore, which in turn, yields an asymmetric charge density in the PE layer, as seen in Figure 2-3(a).

If $V_{\text{applied}} > 0$, the applied electric field drives cations (anions) to the upper (lower) reservoir. The positively charged PE layer of the nanopore makes it difficult for K^+ to migrate through the nanopore, and its concentration in the nanopore decreases accordingly. However, due to the applied pH gradient, the concentration of H^+ in the nanopore remains appreciable. This is because for $V_{\text{applied}} > 0$, the direction of H^+ diffusion driven by the pH gradient is the same as that driven by V_{applied} and the diffusivity of H^+ is large. Note that as shown in Figure 2-3(a), although the nanopore is positively charged, H^+ can still be driven into the nanopore so that the charge density of the nanopore ρ_m increases. If V_{applied} is sufficiently large, no additional H^+ can be driven into the nanopore because of a higher ρ_m . The increase in ρ_m due to the increase in V_{applied} becomes insignificant, as presented in Figure 2-3(a) (diamond and triangle symbols). If a nanopore is positively charged, the electric attraction yields an enrichment in anions inside the nanopore. Since ρ_m does not vary significantly with positive V_{applied} , this enrichment is inappreciable, as shown in Figure 2-S2(a). Because the ionic concentration distribution in the nanopore remains essentially the same, so is G .

For the case of $V_{\text{applied}} < 0$, H^+ is driven by V_{applied} leaving the region near the



lower opening of the nanopore, but at the same time it is driven into the nanopore by the applied pH gradient. If $|V_{\text{applied}}|$ is small (e.g., $V_{\text{applied}} = -0.2 \text{ V}$), the driving force coming from the applied pH gradient is offset slightly by that from the applied electric field so that a less amount of H^+ diffuses from lower side reservoir into the nanopore. As a result, the concentration of H^+ inside the nanopore decreases when V_{applied} changes from 0 to -0.2 V , so does ρ_m (as seen in Figure 2-3(a)). It is worth noting that because the ρ_m of the upper side of the nanopore nearly vanishes (i.e., uncharged) so that more amount of K^+ can be driven into the nanopore. This lowers the concentration of H^+ , and therefore, ρ_m . Furthermore, at a higher $|V_{\text{applied}}|$ (e.g., $V_{\text{applied}} = -0.5 \text{ V}$), the driving force coming from the applied electric field is much stronger than that from the applied pH gradient. A stronger electric field drives more amount of K^+ from the upper reservoir into the nanopore and, at the same time, the solution in the upper reservoir having a high pH (low H^+ concentration) is also driven into the nanopore by EOF. The concentration of H^+ in the nanopore decreases significantly, which makes the pH inside it higher than IEP. Therefore, the sign of ρ_m changes from positive to negative, and $|\rho_m|$ increases appreciably, as seen in Figure 2-3(a) (red dashed line). A larger $|\rho_m|$ can attract more amount of ions, thereby raising the ion concentration in the nanopore, as shown in Figure 2-4(a), and G increases significantly for $V_{\text{applied}} < 0$.

2-3-2 Conductance at $\text{pH}_\text{H}/\text{pH}_\text{L}=7/3$

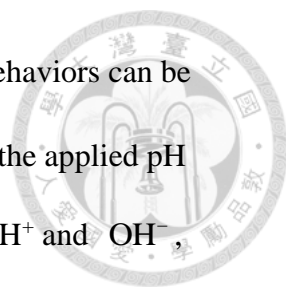
At $\text{pH}_\text{H}/\text{pH}_\text{L}=7/3$, $G(V_{\text{applied}} < 0)$ is insensitive to the variation of $|V_{\text{applied}}|$, while $G(V_{\text{applied}} > 0)$ changes slightly with increasing $|V_{\text{applied}}|$. Similar to that of the case at $\text{pH}_\text{H}/\text{pH}_\text{L}=11/3$, the behavior of $G(V_{\text{applied}} > 0)$ at $\text{pH}_\text{H}/\text{pH}_\text{L}=7/3$ can be explained by the

axial variation in the cross sectional averaged ion distribution shown in Figure 2-S2(b), where that distribution (and therefore, G) varies slightly with increasing V_{applied} .

If $V_{\text{applied}} < 0$, although the driving force coming from the applied electric field is stronger at a higher V_{applied} (e.g., $V_{\text{applied}} = -0.5 \text{ V}$), because the pH of the solution driven into the nanopore is 7 the concentration of H^+ inside it will not decrease as significantly as that when $\text{pH}_\text{H}/\text{pH}_\text{L}=11/3$. The solution pH in the lower part of the nanopore is higher than IEP, and that in its upper part lower than IEP. As a result, the nanopore becomes bi-polar, that is, its lower part is positively charged and upper part negatively charged, with the charge density of the latter lower than that of the former, as seen in Figure 2-3(b). Compared to that at $\text{pH}_\text{H}/\text{pH}_\text{L}=11/3$, the positive ρ_m at $\text{pH}_\text{H}/\text{pH}_\text{L}=7/3$ is smaller, so is the amount of Cl^- attracted into the nanopore. However, Figure 2-3(b) reveals that as V_{applied} varies from -0.2 to -0.5 V , the sign of ρ_m of the upper part of the nanopore changes from positive to negative, and the concentration of K^+ in the nanopore increases. These make the increase in the total amount of ions in the nanopore as V_{applied} varies from -0.2 to -0.5 V inappreciable (as seen in Figure 2-4(b)), so is G .

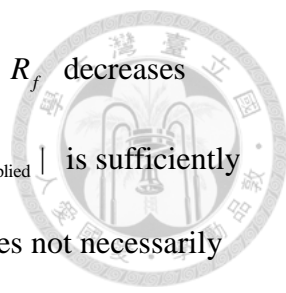
2-3-3 Current Rectifying Behavior at $\text{pH}_\text{H}/\text{pH}_\text{L}=11/3$

The influence of V_{applied} on the ICR factor R_f is shown in Figure 2-5. The present cylindrical nanopore functionalized with single PE brushes shows ICR behavior. For the levels of N_{total} examined, it is interesting to see that at $\text{pH}_\text{H}/\text{pH}_\text{L}=11/3$ if $|V_{\text{applied}}|$ is small, $R_f < 1$, that is, $|I(V_{\text{applied}} > 0)| > |I(V_{\text{applied}} < 0)|$ or the ionic current prefers positive V_{applied} . In contrast, if $|V_{\text{applied}}|$ is sufficiently large, $R_f > 1$, that is,



$|I(V_{\text{applied}} > 0)| < |I(V_{\text{applied}} < 0)|$ or it prefers negative V_{applied} . These behaviors can be attributed to the competition between the driving force coming from the applied pH gradient and that from the charge of the nanopore PE layer. For both H^+ and OH^- , since the direction of diffusion driven by the applied pH gradient is the same as that driven by V_{applied} when $V_{\text{applied}} > 0$, their concentrations are appreciably higher than those when $V_{\text{applied}} < 0$ (Figure 2-6(a) and (c)). However, if $|V_{\text{applied}}|$ is small (e.g., $|V_{\text{applied}}| = 0.2 \text{ V}$), the concentrations of K^+ and Cl^- at $V_{\text{applied}} < 0$ are higher than those at $V_{\text{applied}} > 0$ (Figure 2-S3(a) and (c)). Figure 2-6(a), (c) and Figure 2-S3(a), (c) show that as V_{applied} varies from 0.2 V to -0.2 V , the decreases in the concentrations of H^+ and OH^- are more significant than the increases in the concentrations K^+ and Cl^- . In addition, because the diffusivities of H^+ and OH^- are much larger than those of K^+ and Cl^- , $I(0.2 \text{ V}) > I(-0.2 \text{ V})$ so that $R_f < 1$.

A comparison of Figure 2-4(a) with Figure 2-S2(a) reveals that if $|V_{\text{applied}}|$ is sufficiently large (e.g., $|V_{\text{applied}}| = 0.5 \text{ V}$), $|\rho_m|(V_{\text{applied}} < 0)$ is ca. 7 times larger than $|\rho_m|(V_{\text{applied}} > 0)$ so that the concentration of ions at $V_{\text{applied}} < 0$ is much higher than that at $V_{\text{applied}} > 0$. Therefore, $I(V_{\text{applied}} < 0)$ is much larger than $I(V_{\text{applied}} > 0)$, yielding $R_f > 1$. At $\text{pH}_\text{H}/\text{pH}_\text{L} = 11/3$ and $|V_{\text{applied}}| = 0.5 \text{ V}$, the difference between the concentration of H^+ (OH^-) for $V_{\text{applied}} > 0$ and that for $V_{\text{applied}} < 0$ is much less appreciable compared with that caused by ρ_m . We conclude that at $\text{pH}_\text{H}/\text{pH}_\text{L} = 11/3$ if $|V_{\text{applied}}|$ is small, the rectifying behavior of the nanopore is dominated by the applied pH gradient, leading to $R_f < 1$, and by the charge of the PE layer if $|V_{\text{applied}}|$ is sufficiently large, yielding $R_f > 1$.



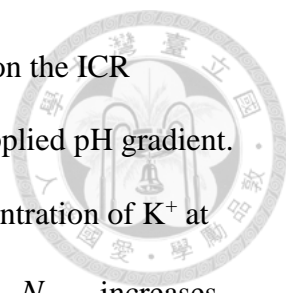
It is interesting to see in Figure 2-5(a) that if $|V_{\text{applied}}|$ is small, R_f decreases with increasing N_{total} , but it increases with increasing N_{total} if $|V_{\text{applied}}|$ is sufficiently large. That is, raising the surface number density of the PE chains does not necessarily improve the ICR performance of the nanopore. This behavior can also be explained by the result of competition between the applied pH gradient and the charge density of the PE layer. As mentioned previously, the applied pH gradient dominates at smaller values of $|V_{\text{applied}}|$. A comparison between Figures 2-3(a) and 2-S4(a) reveals that if N_{total} is raised from 0.1 to 0.5 chains/nm², $|\rho_m|$ increases ca. 3 times, and its influence on the ICR behavior of the nanopore is enhanced. Although an increase in ρ_m makes the difference between the concentration of H⁺ at $V_{\text{applied}} > 0$ and that at $V_{\text{applied}} < 0$ smaller, this effect is still less significant than that of the applied pH gradient. The domination of the pH gradient results in $R_f < 1$. For example, $R_f(N_{\text{total}} = 0.5) \cong 1.26 R_f(N_{\text{total}} = 0.1)$ at $|V_{\text{applied}}| = 0.2$ V; note that, however, both are smaller than unity. For larger values of $|V_{\text{applied}}|$, the ICR behavior of the nanopore (or R_f) is dominated by ρ_m . As mentioned previously, $|\rho_m(N_{\text{total}} = 0.5)| \cong 3|\rho_m(N_{\text{total}} = 0.1)|$. Figures 2-3 and 2-S4 indicate that the degree of increase in $|\rho_m|(V_{\text{applied}} < 0)$ as N_{total} increases from 0.1 to 0.5 chains/nm² is much more appreciable than that in $|\rho_m|(V_{\text{applied}} > 0)$. This makes the increase in the concentration of ions for $V_{\text{applied}} < 0$ appreciable, but that for $V_{\text{applied}} > 0$ less appreciable. Therefore, if $|V_{\text{applied}}|$ is sufficiently large, R_f increases with increasing N_{total} , showing a stronger preference for $V_{\text{applied}} < 0$. In this case, R_f increases by ca. 2 to 3 times when N_{total} is raised from 0.1 to 0.5 chains/nm². Recall that as N_{total} increases from 0.1 to 0.5 chains/nm², R_f increases only ca. 1.26 times when $|V_{\text{applied}}|$

is small. These suggest that the ICR behavior of the nanopore at a high level of $|V_{\text{applied}}|$ is more sensitive to the grafting density of its PE chains than that at a low level of $|V_{\text{applied}}|$. We conclude that whether the ICR behavior of the nanopore is dominated by the charge density of its PE layer or by the applied pH gradient depends mainly on the level of the applied voltage.

2-3-4 Current Rectifying Behavior at $\text{pH}_\text{H}/\text{pH}_\text{L}=7/3$

Figure 2-5(b) reveals that at $\text{pH}_\text{H}/\text{pH}_\text{L}=7/3$ and $N_{\text{total}} = 0.1 \text{ chains/nm}^2$, $R_f < 1$ for the range of V_{applied} examined. At this level of pH gradient the increase in the charge density of the PE layer with V_{applied} is not that significant compared with that at $\text{pH}_\text{H}/\text{pH}_\text{L}=11/3$. As shown in Figure 2-3(b) that at $V_{\text{applied}} = -0.5 \text{ V}$ the upper part of the nanopore is only slightly negatively charged. Although $|V_{\text{applied}}|$ is large (e.g., $V_{\text{applied}} = -0.5 \text{ V}$), the driving force coming from the applied pH gradient is greater than that from the charge density. Because H^+ is driven by its concentration gradient and by a positive V_{applied} towards the same direction, its concentration in the nanopore is higher than that for the corresponding negative V_{applied} . For example, Figure 2-S5(a) shows that the concentration of H^+ at $V_{\text{applied}} = 0.5 \text{ V}$ is higher than that $V_{\text{applied}} = -0.5 \text{ V}$. This implies that $I(V_{\text{applied}} > 0)$ is larger than $I(V_{\text{applied}} < 0)$, yielding $R_f < 1$.

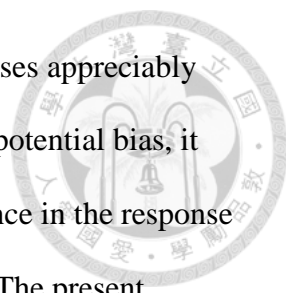
If the grafting density of the PE layer N_{total} is raised from 0.1 to 0.5 chains/nm², R_f exceeds unity, implying that the preferential of current direction can be reversed by tuning the grafting density of the PE layer. Note that the higher the grafting density of the PE layer the higher is its charge density. Therefore, if the grafting density is



sufficiently high, the influence of the charge density of the PE layer on the ICR behavior of the nanopore becomes more important than that of the applied pH gradient. As shown in Figure 2-S6(a) and (b) the difference between the concentration of K^+ at $V_{\text{applied}} = 0.5 \text{ V}$ and that at $V_{\text{applied}} = -0.5 \text{ V}$ increases appreciably as N_{total} increases from 0.1 to 0.5 chains/nm². Note that at $N_{\text{total}} = 0.5 \text{ chains/nm}^2$ the difference between the concentration of H^+ for $V_{\text{applied}} > 0$ and that for $V_{\text{applied}} < 0$ is inappreciable, neither is the difference between the concentration of Cl^- for $V_{\text{applied}} > 0$ and that for $V_{\text{applied}} < 0$. The former implies that the influence of the applied pH gradient is insignificant. The latter arises from that the sign of the charge of the nanopore PE layer changes from positive to negative as V_{applied} varies from 0.5 V to -0.5 V. The negative charge carried by the nanopore for $V_{\text{applied}} < 0$ is appreciable, thereby attracting a consider amount of K^+ , yielding a current which is greater than that for $V_{\text{applied}} > 0$ V so that $R_f > 1$. Therefore, through applying a moderate strength of pH gradient, the preferred current direction can be switched by varying the grafting density of the PE layer.

2-4. Conclusions

Taking account of the effects of the pH-regulated nature of a cylindrical nanopore surface functionalized with polyelectrolyte (PE) brushes and the presence of electroosmotic flow, this study investigates the influence of applying an extra pH gradient in addition to an electric field on the ionic transport in the nanopore. It is interesting to see that if the applied pH gradient is sufficiently strong, the nanopore conductance exhibits disparate response to the applied potential bias, depending upon



its sign. For negatively applied potential bias, the conductance increases appreciably with the increase in the applied potential bias; for positively applied potential bias, it becomes insensitive to that bias. This can be attributed to the difference in the response of the charge density of the PE brushes to the applied potential bias. The present cylindrical nanopore is able to exhibit ion current rectification (ICR) behavior that is usually seen in geometrically asymmetric nanopores. For a fixed strength of the applied pH gradient, the ICR factor measuring the degree of ICR of the nanopore can be tuned by the applied potential bias. A rectification inversion is observed when the applied potential bias is ca. ± 0.3 V. Depending on the level of the applied potential bias, the ICR behavior of the nanopore is dominated either by the applied pH gradient or by the charge density of the PE brushes. The rectification inversion can also be observed at a moderate pH gradient strength when the grafting density of the PE brushes is raised from 0.1 to 0.5 chains/nm². The results obtained in this study reveal that the ionic transport in the nanopore can be influenced significantly by the applied pH gradient. Together with the key factors including the nanopore geometry and the way that nanopore surface is modified, we conclude that applying such a gradient can be a promising approach for improving the ICR performance of the nanopore.

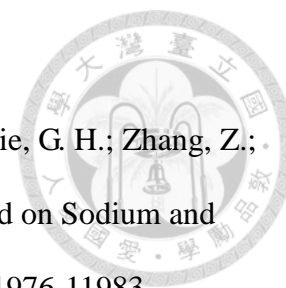



References

1. Zhang, Y.; Schatz, G. C. Conical Nanopores for Efficient Ion Pumping and Desalination. *J. Phys. Chem. Lett.* **2017**, *8*, 2842-2848.
2. Zhang, H. C.; Hou, X.; Zeng, L.; Yang, F.; Li, L.; Yan, D. D.; Tian, Y.; Jiang, L. Bioinspired Artificial Single Ion Pump. *J. Am. Chem. Soc.* **2013**, *135*, 16102-16110.
3. Wu, X. J.; Rajasekaran, P. R.; Martin, C. R. An Alternating Current Electroosmotic Pump Based on Conical Nanopore Membranes. *ACS Nano* **2016**, *10*, 4637-4643.
4. Zhang, Z.; Sui, X.; Li, P.; Xie, G. H.; Kong, X. Y.; Xiao, K.; Gao, L. C.; Wen, L. P.; Jiang, L. Ultrathin and Ion-Selective Janus Membranes for High-Performance Osmotic Energy Conversion. *J. Am. Chem. Soc.* **2017**, *139*, 8905-8914.
5. Hsu, J. P.; Lin, S. C.; Lin, C. Y.; Tseng, S. Power Generation by a pH-Regulated Conical Nanopore through Reverse Electrodialysis. *J. Power Sources* **2017**, *366*, 169-177.
6. Yeh, L. H.; Chen, F.; Chiou, Y. T.; Su, Y. S. Anomalous pH-Dependent Nanofluidic Salinity Gradient Power. *Small* **2017**, *13*, 1702691.
7. Hwang, J.; Sekimoto, T.; Hsu, W. L.; Kataoka, S.; Endo, A.; Daiguji, H. Thermal Dependence of Nanofluidic Energy Conversion by Reverse Electrodialysis. *Nanoscale* **2017**, *9*, 12068-12076.
8. Tseng, S.; Li, Y. M.; Lin, C. Y.; Hsu, J. P. Salinity Gradient Power: Influences of Temperature and Nanopore Size. *Nanoscale* **2016**, *8*, 2350-2357.
9. Buchsbaum, S. F.; Nguyen, G.; Howorka, S.; Siwy, Z. S. DNA-Modified Polymer Pores Allow pH- and Voltage-Gated Control of Channel Flux. *J. Am. Chem. Soc.* **2014**, *136*, 9902-9905.
10. Zhang, H. C.; Tian, Y.; Hou, J.; Hou, X.; Hou, G. L.; Ou, R. W.; Wang, H. T.; Jiang, L. Bioinspired Smart Gate-Location-Controllable Single Nanochannels: Experiment and

Theoretical Simulation. *ACS Nano* **2015**, *9*, 12264-12273.

11. Liu, Q.; Xiao, K.; Wen, L. P.; Lu, H.; Liu, Y. H.; Kong, X. Y.; Xie, G. H.; Zhang, Z.; Bo, Z. S.; Jiang, L. Engineered Ionic Gates for Ion Conduction Based on Sodium and Potassium Activated Nanochannels. *J. Am. Chem. Soc.* **2015**, *137*, 11976-11983.
12. Ali, M.; Nasir, S.; Ramirez, P.; Cervera, J.; Mafe, S.; Ensinger, W. Calcium Binding and Ionic Conduction in Single Conical Nanopores with Polyacid Chains: Model and Experiments. *ACS Nano* **2012**, *6*, 9247-9257.
13. Mayne, L.; Lin, C. Y.; Christie, S. D. R.; Siwy, Z. S.; Platt, M. The Design and Characterization of Multifunctional Aptamer Nanopore Sensors. *ACS Nano* **2018**, *12*, 4844-4852.
14. Mayne, L. J.; Christie, S. D. R.; Platt, M. A Tunable Nanopore Sensor for the Detection of Metal Ions Using Translocation Velocity and Biphasic Pulses. *Nanoscale* **2016**, *8*, 19139-19147.
15. Hemmig, E. A.; Fitzgerald, C.; Maffeo, C.; Hecker, L.; Ochmann, S. E.; Aksimentiev, A.; Tinnefeld, P.; Keyser, U. F. Optical Voltage Sensing Using DNA Origami. *Nano Lett.* **2018**, *18*, 1962-1971.
16. Heerema, S. J.; Vicarelli, L.; Pud, S.; Schouten, R. N.; Zandbergen, H. W.; Dekker, C. Probing DNA Translocations with Inplane Current Signals in a Graphene Nanoribbon with a Nanopore. *ACS Nano* **2018**, *12*, 2623-2633.
17. Cao, C.; Ying, Y. L.; Hu, Z. L.; Liao, D. F.; Tian, H.; Long, Y. T. Discrimination of Oligonucleotides of Different Lengths with a Wild-Type Aerolysin Nanopore. *Nat. Nanotech.* **2016**, *11*, 713-718.
18. Vlasiouk, I.; Smirnov, S.; Siwy, Z. Ionic Selectivity of Single Nanochannels. *Nano Lett.* **2008**, *8*, 1978-1985.
19. Yeh, L. H.; Hughes, C.; Zeng, Z. P.; Qian, S. Z. Tuning Ion Transport and



- 
- Selectivity by a Salt Gradient in a Charged Nanopore. *Anal. Chem.* **2014**, *86*, 2681-2686.
20. White, H. S.; Bund, A. Ion Current Rectification at Nanopores in Glass Membranes. *Langmuir* **2008**, *24*, 2212-2218.
21. Plett, T.; Le Thai, M.; Cai, J.; Vlasiouk, I.; Penner, R. M.; Siwy, Z. S. Ion Transport in Gel and Gel-Liquid Systems for LiClO₄-Doped Pmma at the Meso- and Nanoscales. *Nanoscale* **2017**, *9*, 16232-16243.
22. Lin, C. Y.; Yeh, L. H.; Siwy, Z. S. Voltage-Induced Modulation of Ionic Concentrations and Ion Current Rectification in Mesopores with Highly Charged Pore Walls. *J. Phys. Chem. Lett.* **2018**, *9*, 393-398.
23. Yameen, B.; Ali, M.; Neumann, R.; Ensinger, W.; Knoll, W.; Azzaroni, O. Synthetic Proton-Gated Ion Channels Via Single Solid-State Nanochannels Modified with Responsive Polymer Brushes. *Nano Lett.* **2009**, *9*, 2788-2793.
24. Zhang, H. C.; Hou, X.; Hou, J.; Zeng, L.; Tian, Y.; Li, L.; Jiang, L. Synthetic Asymmetric-Shaped Nanodevices with Symmetric pH-Gating Characteristics. *Adv. Funct. Mater.* **2015**, *25*, 1102-1110.
25. Perez-Mitta, G.; Burr, L.; Tuninetti, J. S.; Trautmann, C.; Toimil-Molares, M. E.; Azzaroni, O. Noncovalent Functionalization of Solid-State Nanopores Via Self-Assembly of Amphipols. *Nanoscale* **2016**, *8*, 1470-1478.
26. Zhang, Z.; Li, P.; Kong, X. Y.; Xie, G. H.; Qian, Y. C.; Wang, Z. Q.; Tian, Y.; Wen, L. P.; Jiang, L. Bioinspired Heterogeneous Ion Pump Membranes: Unidirectional Selective Pumping and Controllable Gating Properties Stemming from Asymmetric Ionic Group Distribution. *J. Am. Chem. Soc.* **2018**, *140*, 1083-1090.
27. Lin, C. Y.; Hsu, J. P.; Yeh, L. H. Rectification of Ionic Current in Nanopores Functionalized with Bipolar Polyelectrolyte Brushes. *Sens. Actuators, B* **2018**, *258*,

1223-1229.

28. Hsu, J. P.; Wu, H. H.; Lin, C. Y.; Tseng, S. Importance of Polyelectrolyte Modification for Rectifying the Ionic Current in Conically Shaped Nanochannels. *Phys. Chem. Chem. Phys.* **2017**, *19*, 5351-5360.

29. Tagliazucchi, M.; Rabin, Y.; Szleifer, I. Transport Rectification in Nanopores with Outer Membranes Modified with Surface Charges and Polyelectrolytes. *ACS Nano* **2013**, *7*, 9085-9097.

30. Yeh, L. H.; Zhang, M.; Qian, S.; Hsu, J. P.; Tseng, S. Ion Concentration Polarization in Polyelectrolyte-Modified Nanopores. *J. Phys. Chem. C* **2012**, *116*, 8672-8677.

31. Yeh, L. H.; Zhang, M. K.; Hu, N.; Joo, S. W.; Qian, S. Z.; Hsu, J. P. Electrokinetic Ion and Fluid Transport in Nanopores Functionalized by Polyelectrolyte Brushes. *Nanoscale* **2012**, *4*, 5169-5177.

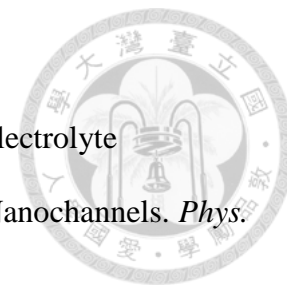
32. Ramirez, P.; Apel, P. Y.; Cervera, J.; Mafe, S. Pore Structure and Function of Synthetic Nanopores with Fixed Charges: Tip Shape and Rectification Properties. *Nanotechnology* **2008**, *19*, 315707.

33. Xiao, K.; Chen, L.; Xie, G. H.; Li, P.; Kong, X. Y.; Wen, L. P.; Jiang, L. A Bio-Inspired Dumbbell-Shaped Nanochannel with a Controllable Structure and Ionic Rectification. *Nanoscale* **2018**, *10*, 6850-6854.

34. Daiguji, H.; Oka, Y.; Shirono, K. Nanofluidic Diode and Bipolar Transistor. *Nano Lett.* **2005**, *5*, 2274-2280.

35. Lin, C. Y.; Yeh, L. H.; Hsu, J. P.; Tseng, S. Regulating Current Rectification and Nanoparticle Transport through a Salt Gradient in Bipolar Nanopores. *Small* **2015**, *11*, 4594-4602.

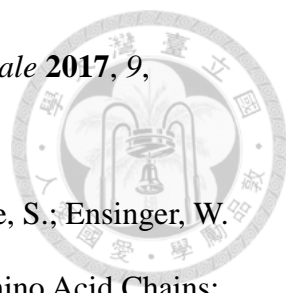
36. Perez-Mitta, G.; Albesa, A. G.; Knoll, W.; Trautmann, C.; Toimil-Molares, M. E.;



Azzaroni, O. Host-Guest Supramolecular Chemistry in Solid-State Nanopores: Potassium-Driven Modulation of Ionic Transport in Nanofluidic Diodes. *Nanoscale* **2015**, *7*, 15594-15598.



37. Hsu, J. P.; Lin, T. W.; Lin, C. Y.; Tseng, S. Salt-Dependent Ion Current Rectification in Conical Nanopores: Impact of Salt Concentration and Cone Angle. *J. Phys. Chem. C* **2017**, *121*, 28139-28147.
38. He, X. L.; Zhang, K. L.; Liu, Y.; Wu, F.; Yu, P.; Mao, L. Q. Chaotropic Monovalent Anion-Induced Rectification Inversion at Nanopipettes Modified by Polyimidazolium Brushes. *Angew. Chem., Int. Ed.* **2018**, *57*, 4590-4593.
39. Cao, L. X.; Guo, W.; Wang, Y. G.; Jiang, L. Concentration-Gradient-Dependent Ion Current Rectification in Charged Conical Nanopores. *Langmuir* **2012**, *28*, 2194-2199.
40. Lin, J. Y.; Lin, C. Y.; Hsu, J. P.; Tseng, S. Ionic Current Rectification in a pH-Tunable Polyelectrolyte Brushes Functionalized Conical Nanopore: Effect of Salt Gradient. *Anal. Chem.* **2016**, *88*, 1176-1187.
41. Taghipoor, M.; Bertsch, A.; Renaud, P. Thermal Control of Ionic Transport and Fluid Flow in Nanofluidic Channels. *Nanoscale* **2015**, *7*, 18799-18804.
42. Ali, M.; Ramirez, P.; Mafe, S.; Neumann, R.; Ensinger, W. A pH-Tunable Nanofluidic Diode with a Broad Range of Rectifying Properties. *ACS Nano* **2009**, *3*, 603-608.
43. Yeh, L. H.; Zhang, M. K.; Qian, S. Z. Ion Transport in a pH-Regulated Nanopore. *Anal. Chem.* **2013**, *85*, 7527-7534.
44. Zeng, Z. P.; Ai, Y.; Qian, S. Z. pH-Regulated Ionic Current Rectification in Conical Nanopores Functionalized with Polyelectrolyte Brushes. *Phys. Chem. Chem. Phys.* **2014**, *16*, 2465-2474.
45. Zheng, Y. B.; Zhao, S.; Cao, S. H.; Cai, S. L.; Cai, X. H.; Li, Y. Q. A Temperature,

- 
- pH and Sugar Triple-Stimuli-Responsive Nanofluidic Diode. *Nanoscale* **2017**, *9*, 433-439.
46. Ali, M.; Ramirez, P.; Nguyen, H. Q.; Nasir, S.; Cervera, J.; Mafe, S.; Ensinger, W. Single Cigar-Shaped Nanopores Functionalized with Amphoteric Amino Acid Chains: Experimental and Theoretical Characterization. *ACS Nano* **2012**, *6*, 3631-3640.
47. Zeng, Z. P.; Yeh, L. H.; Zhang, M. K.; Qian, S. Z. Ion Transport and Selectivity in Biomimetic Nanopores with pH -Tunable Zwitterionic Polyelectrolyte Brushes. *Nanoscale* **2015**, *7*, 17020-17029.
48. Alcaraz, A.; Ramirez, P.; Garcia-Gimenez, E.; Lopez, M. L.; Andrio, A.; Aguilera, V. M. A pH -Tunable Nanofluidic Diode: Electrochemical Rectification in a Reconstituted Single Ion Channel. *J. Phys. Chem. B* **2006**, *110*, 21205-21209.
49. Queralt-Martin, M.; Peiro-Gonzalez, C.; Aguilera-Arzo, M.; Alcaraz, A. Effects of Extreme pH on Ionic Transport through Protein Nanopores: The Role of Ion Diffusion and Charge Exclusion. *Phys. Chem. Chem. Phys.* **2016**, *18*, 21668-21675.
50. Zhang, Z.; Kong, X. Y.; Xiao, K.; Xie, G. H.; Liu, Q.; Tian, Y.; Zhang, H. C.; Ma, J.; Wen, L. P.; Jiang, L. A Bioinspired Multifunctional Heterogeneous Membrane with Ultrahigh Ionic Rectification and Highly Efficient Selective Ionic Gating. *Adv. Mater.* **2016**, *28*, 144-150.
51. Wang, L.; Guo, W.; Xie, Y. B.; Wang, X. W.; Xue, J. M.; Wang, Y. G. Nanofluidic Diode Generated by pH Gradient inside Track-Etched Conical Nanopore. *Radiat. Meas.* **2009**, *44*, 1119-1122.
52. Haywood, D. G.; Harms, Z. D.; Jacobson, S. C. Electroosmotic Flow in Nanofluidic Channels. *Anal. Chem.* **2014**, *86*, 11174-11180.
53. Hsu, J. P.; Yang, S. T.; Lin, C. Y.; Tseng, S. Ionic Current Rectification in a Conical Nanopore: Influences of Electroosmotic Flow and Type of Salt. *J. Phys. Chem. C* **2017**,

121, 4576-4582.

54. Lin, D. H.; Lin, C. Y.; Tseng, S.; Hsu, J. P. Influence of Electroosmotic Flow on the Ionic Current Rectification in a pH-Regulated, Conical Nanopore. *Nanoscale* **2015**, *7*, 14023-14031.

55. Peleg, O.; Tagliacruzchi, M.; Kroger, M.; Rabin, Y.; Szeleifer, I. Morphology Control of Hairy Nanopores. *ACS Nano* **2011**, *5*, 4737-4747.

56. Tagliacruzchi, M.; Rabin, Y.; Szeleifer, I. Ion Transport and Molecular Organization Are Coupled in Polyelectrolyte-Modified Nanopores. *J. Am. Chem. Soc.* **2011**, *133*, 17753-17763.

57. Duval, J. F. L.; Gaboriaud, F. Progress in Electrohydrodynamics of Soft Microbial Particle Interphases. *Curr. Opin. Colloid Interface Sci.* **2010**, *15*, 184-195.

58. Ohshima, H. Electrophoresis of Soft Particles. *Adv. Colloid Interface Sci.* **1995**, *62*, 189-235.

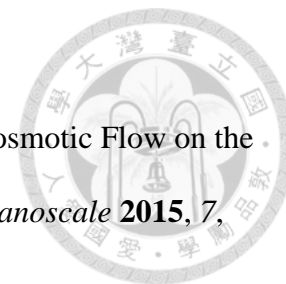
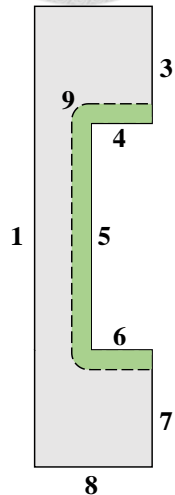


Table 2-1. Boundary conditions assumed for eqs 1-4.

surface	Poisson	Nernst-Planck	Stokes-Brinkman
1	axial symmetry		
2	$\phi = 0$ (grounded)	$C_i = C_{i0}$ (bulk concentration)	$p = 0$ (no external pressure applied)
8	$\phi = V_{\text{applied}}$ (applied voltage)		
3, 7	$-\mathbf{n} \cdot \nabla \phi = 0$ (no accumulated charge)	$\mathbf{n} \cdot \mathbf{J}_i = 0$ (zero normal flux)	slip
4,5,6	$-\mathbf{n} \cdot \nabla \phi = 0$ (uncharged)	$\mathbf{n} \cdot \mathbf{J}_i = 0$ (ion-impenetrable)	$\mathbf{u} = \mathbf{0}$ (nonslip)
9	continuous		



shaded area:
nanopore boundary
(not to scale)

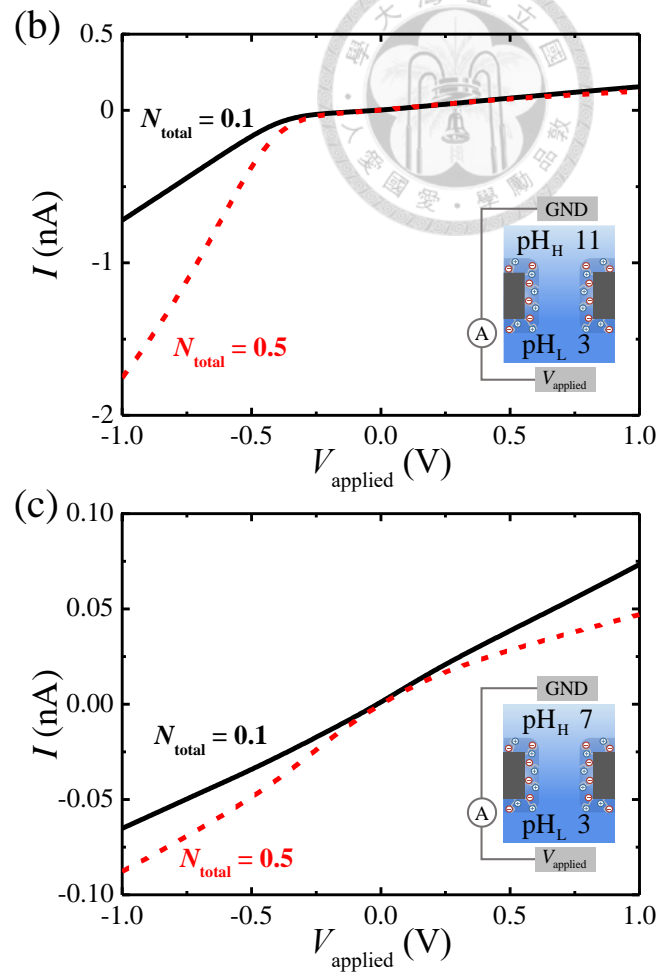
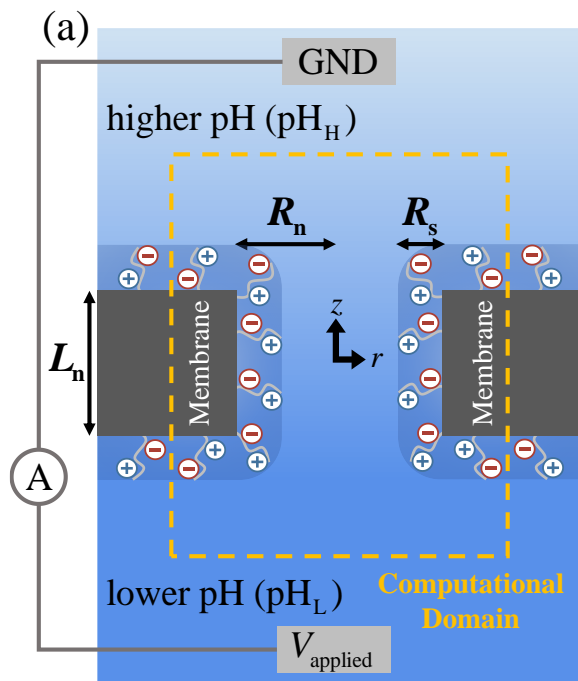


Figure 2-1. (a) Electrokinetic transport of ions in a cylindrical nanopore of radius R_n and axial length L_n surface modified with a PE layer of thickness R_s connecting two large, identical cylindrical reservoirs. The upper reservoir is grounded, and a potential bias V_{applied} is applied to the lower reservoir. A pH gradient is also applied across the nanopore with the bulk pH in the lower and upper reservoirs pH_L and pH_H , respectively. The region enclosed by the dashed rectangle denotes the computational domain considered in the numerical solution. The I - V curves for two levels of N_{total} at $C_{\text{bulk}} = 1 \text{ mM}$. (b) $\text{pH}_H/\text{pH}_L=11/3$, (c) $\text{pH}_H/\text{pH}_L=7/3$. Solid curves: $V_{\text{applied}} < 0$; dashed curves: $V_{\text{applied}} > 0$.

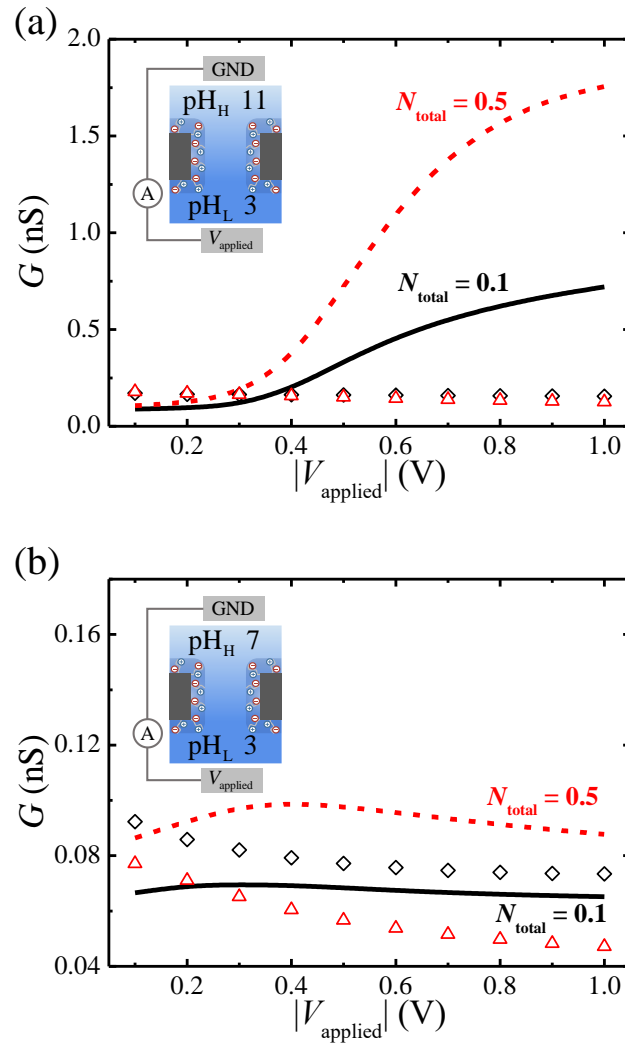


Figure 2-2. Variation of the nanopore conductance G as a function of $|V_{\text{applied}}|$ for two levels of the grafting density of PE chains N_{total} . (a) $\text{pH}_H/\text{pH}_L=11/3$, (b) $\text{pH}_H/\text{pH}_L=7/3$.

Curves: $V_{\text{applied}} < 0$; discrete symbols: $V_{\text{applied}} > 0$.

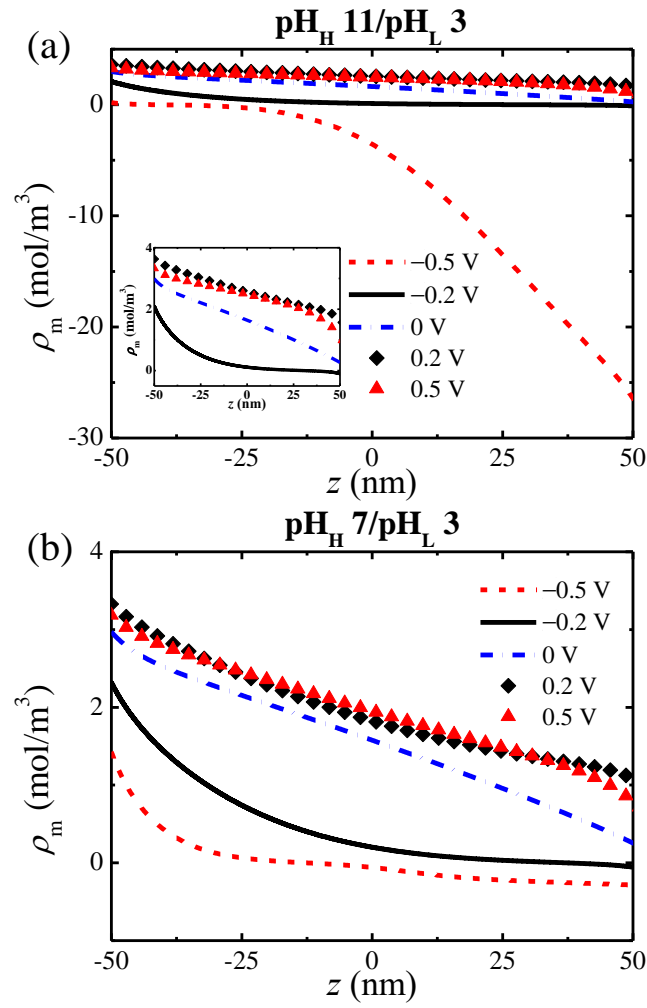


Figure 2-3. Axial variation in the charge density of the PE layer ρ_m for various levels of V_{applied} at $N_{\text{total}} = 0.1$ chains/nm². (a) $\text{pH}_H/\text{pH}_L=11/3$, (b) $\text{pH}_H/\text{pH}_L=7/3$.

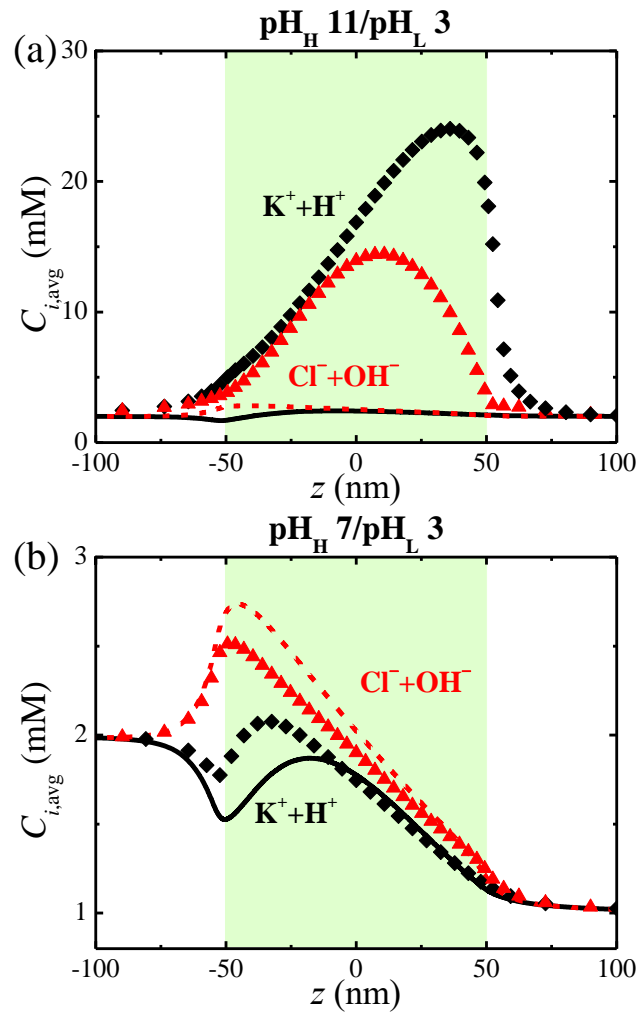


Figure 2-4. Axial variation in the cross sectional averaged concentrations of cations (K^+ and H^+) and anions (Cl^- and OH^-) at $N_{total} = 0.1$ chains/nm². (a) $pH_H/pH_L=11/3$, (b) $pH_H/pH_L=7/3$. Curves: $V_{applied} = -0.2$ V ; discrete symbols: $V_{applied} = -0.5$ V .

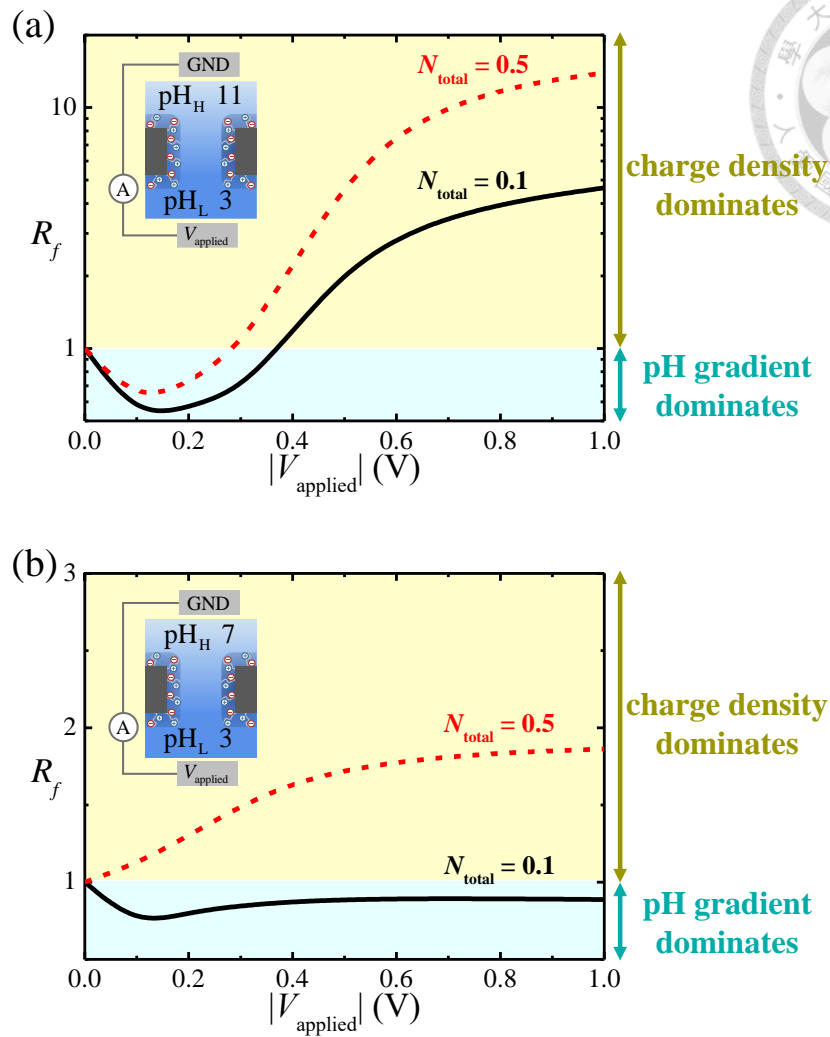


Figure 2-5. ICR factor, $R_f = |I(V_{\text{applied}} < 0) / I(V_{\text{applied}} > 0)|$, as a function of the magnitude of applied voltage bias $|V_{\text{applied}}|$ for two values of N_{total} . (a) $\text{pH}_H/\text{pH}_L=11/3$, (b) $\text{pH}_H/\text{pH}_L=7/3$.

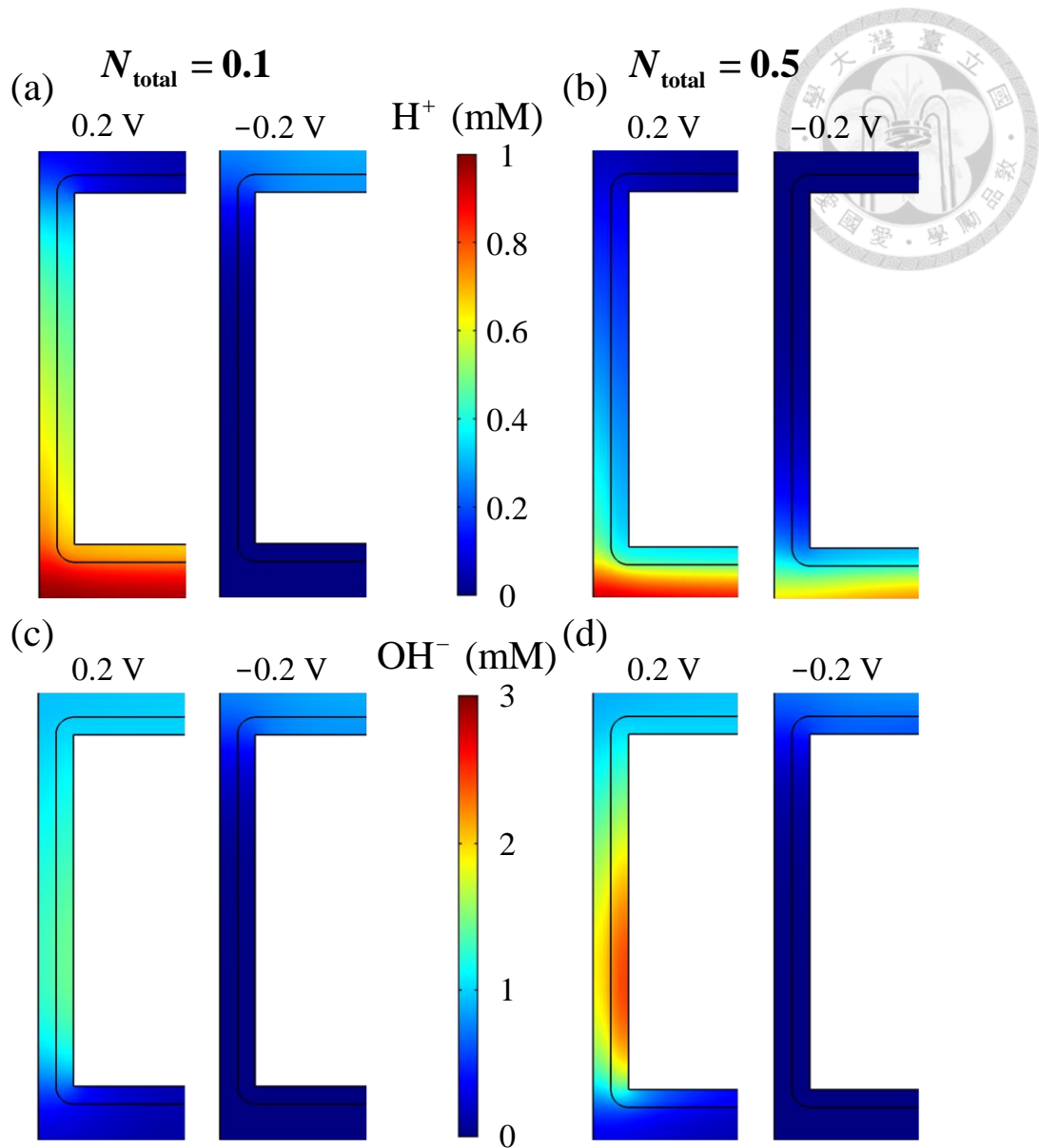


Figure 2-6. Concentration profiles of H^+ , (a) and (b), and OH^- , (c) and (d), for two values of the grafting density of PE chains N_{total} at $\text{pH}_\text{H}/\text{pH}_\text{L}=11/3$.

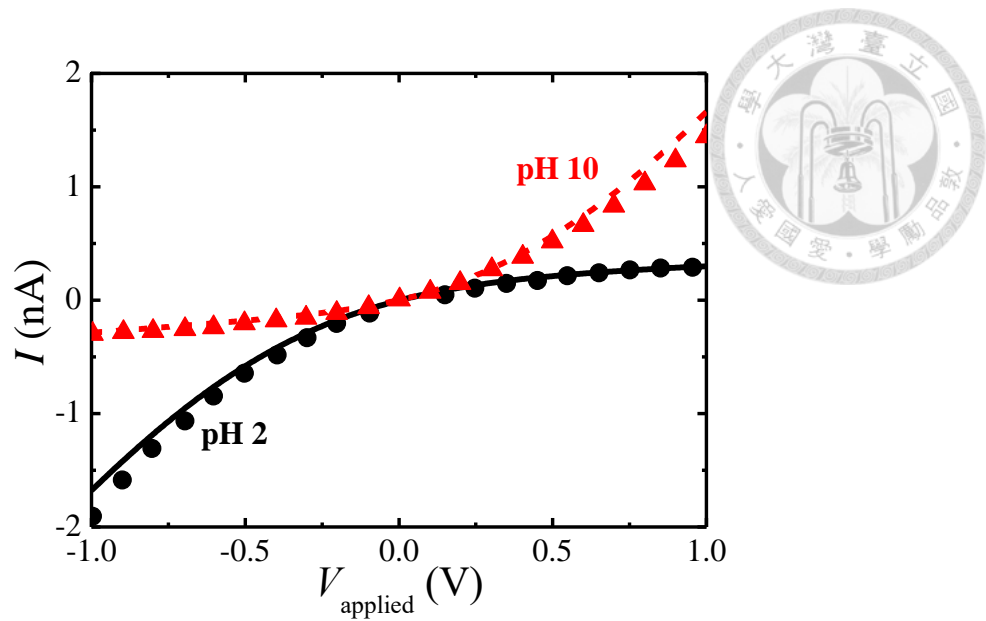


Figure 2-S1. Current-voltage curves of a single polyethylene terephthalate (PET) conical nanopore with its surface functionalized with Lysine in 100 mM KCl solution for various pH values. The pore thickness is 12 μm with tip radius of 8 nm and base radius of 165 nm. The polyelectrolyte layer is assumed 1 nm thick with $\lambda = 0.2 \text{ nm}$.²⁷

⁵⁷ Curves: present theoretical results with variables $\text{pK}_A = 2.2$, $\text{pK}_B = 9$, and $N_{\text{total}} = 0.6 \text{ chains/nm}^2$; discrete symbols: experimental data of Ali et al.⁴²

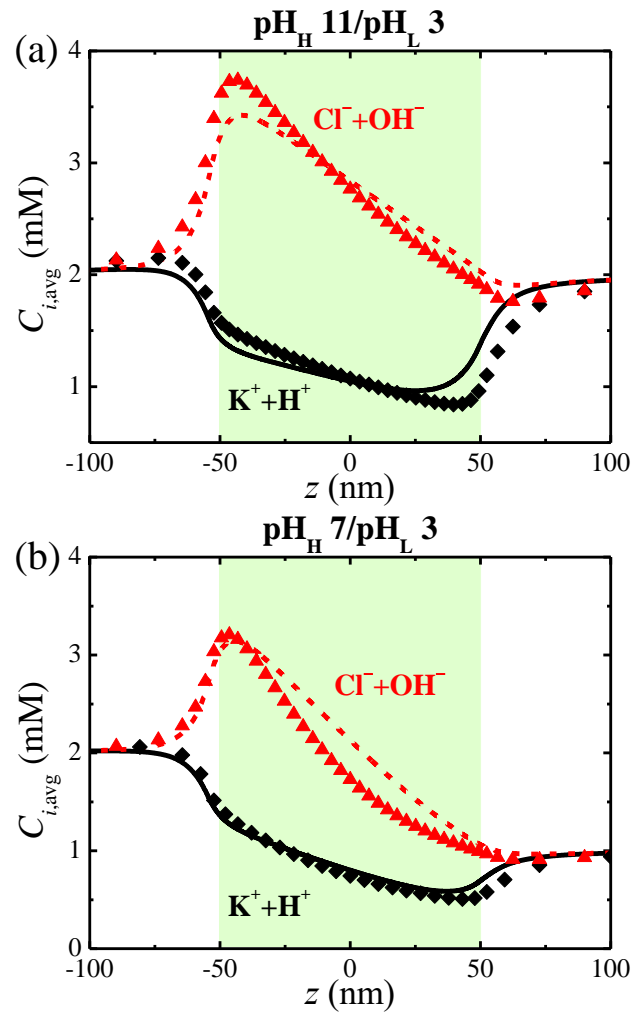


Figure 2-S2. Axial variation in the cross sectional averaged concentrations of cations

(K^+ and H^+) and anions (Cl^- and OH^-) with $N_{\text{total}} = 0.1 \text{ chains/nm}^2$ at

$\text{pH}_H/\text{pH}_L=11/3$, (a), and $\text{pH}_H/\text{pH}_L=7/3$, (b). Curves: $V_{\text{applied}} = 0.2 \text{ V}$; discrete symbols:

$V_{\text{applied}} = 0.5 \text{ V}$.

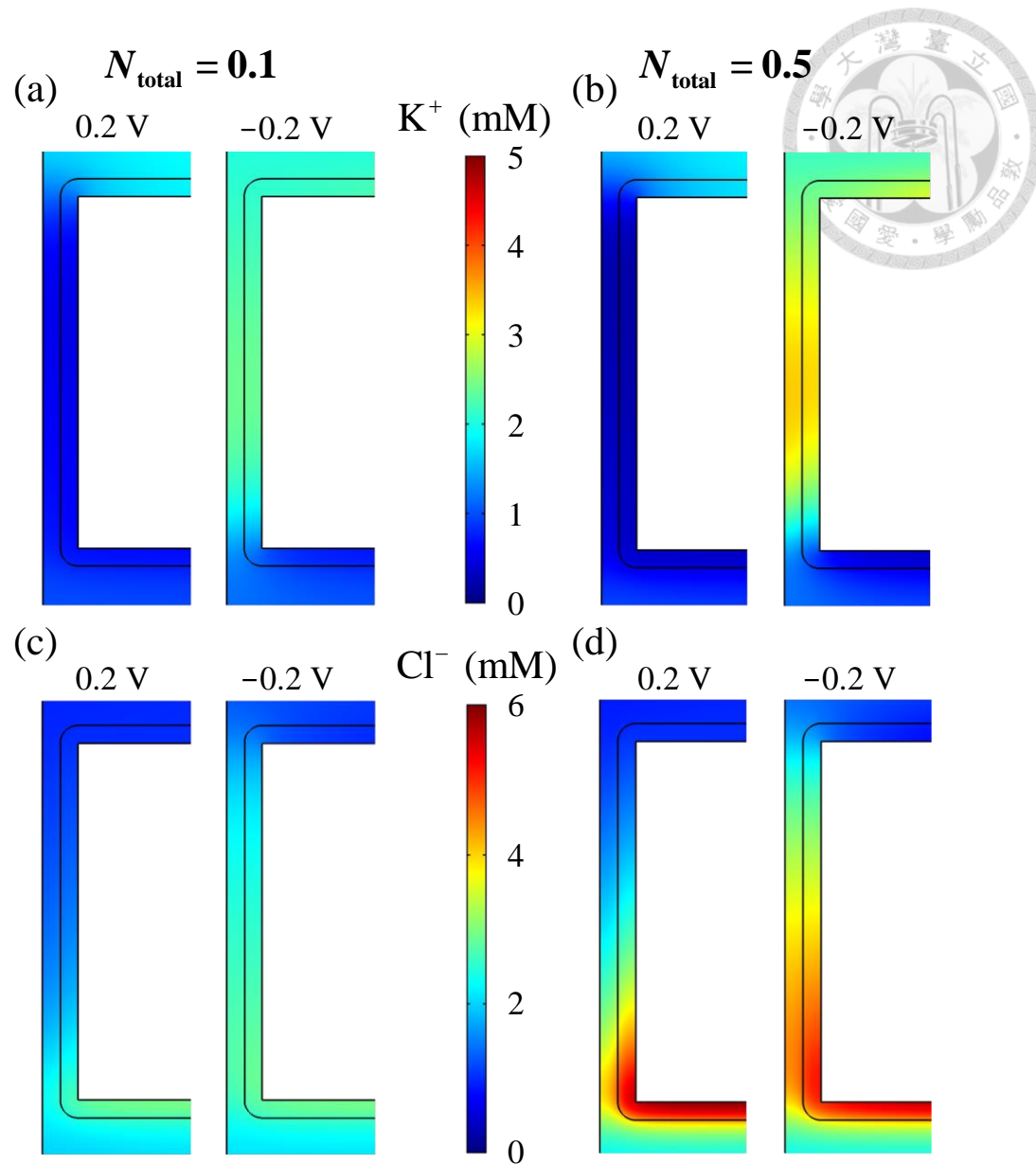


Figure 2-S3. Concentration profiles of K^+ , (a) and (b), and Cl^- , (c) and (d), for two values of the grafting density of PE chains N_{total} at $pH_H/pH_L=11/3$.

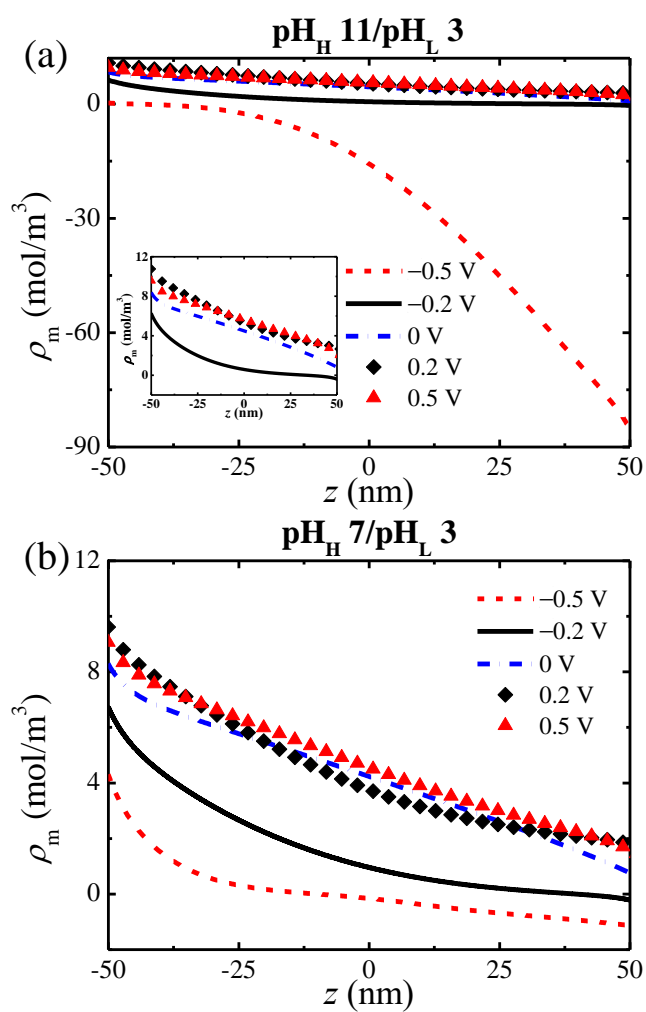


Figure 2-S4. Axial variation in the charge density of the PE layer ρ_m for various levels of V_{applied} with $N_{\text{total}} = 0.5$ chains/nm² at $\text{pH}_H/\text{pH}_L=11/3$, (a), and $\text{pH}_H/\text{pH}_L=7/3$, (b).

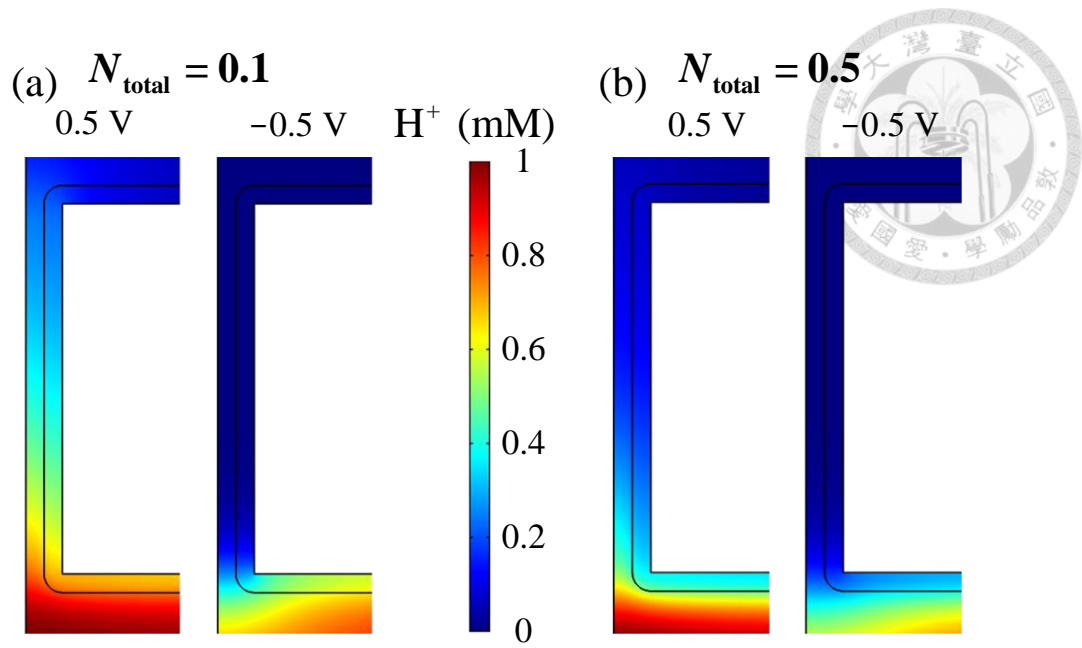


Figure 2-S5. Concentration profiles of H^+ for two values of grafting density of PE chains N_{total} at $\text{pH}_H/\text{pH}_L=7/3$.

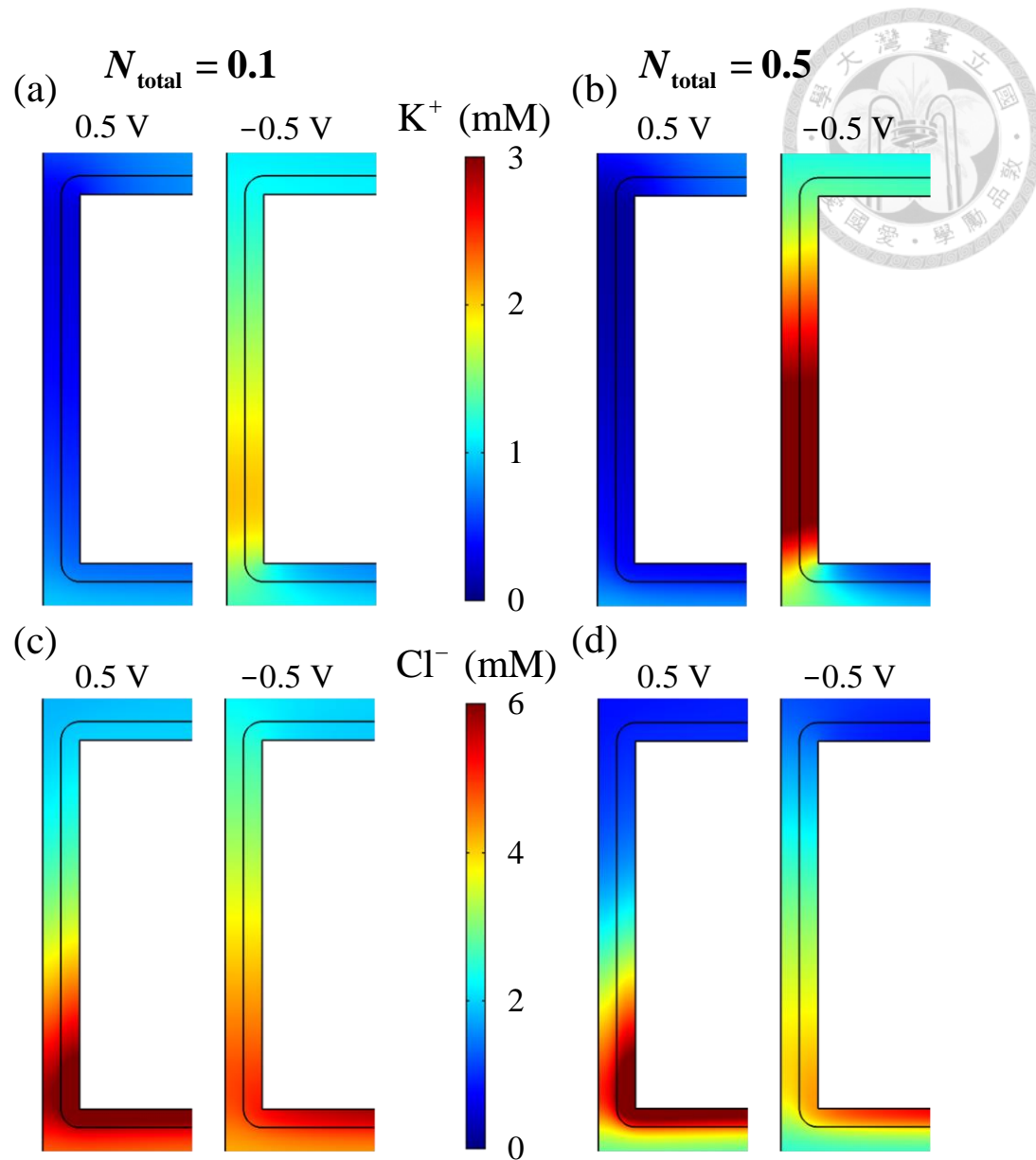


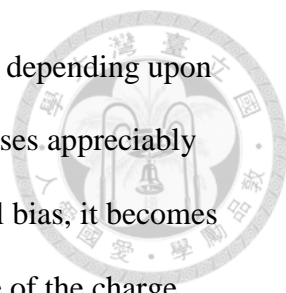
Figure 2-S6. Concentration profiles of K^+ , (a) and (b), and Cl^- , (c) and (d), for two values of the grafting density of PE chains N_{total} at $pH_H/pH_L=7/3$.

Chapter 3 Conclusions



Ion current rectification (ICR) behavior with response to several factors are theoretically investigated in this thesis. Chapter 1 focuses on effects of half cone angle θ , bulk salt concentration C_{bulk} , and type of salt (KCl, NaCl, LiCl) on ICR in negatively charged nanopores. Rectification ratio R_f of three types of salt ranks as $R_f(\text{LiCl}) > R_f(\text{NaCl}) > R_f(\text{KCl})$ at $C_{\text{bulk}} = 3 \text{ mM}$ and/or $\theta < 1^\circ$ for all levels of voltage potential V_0 . The above order can be reversed when nanopores are applied with sufficiently high V_0 at higher C_{bulk} and/or larger θ . As a result, the $R_f - V_0$ curves of the types of salt examined intersect at the same point. This phenomenon results from the different degree of ion enrichment of three types of salt at positive voltage. Degree of enrichment of LiCl is the largest under small voltage regardless of the level of θ ; however, if we increase level of applied voltage, enrichment of KCl becomes the largest only if $\theta > 1^\circ$. We also observed that the point of intersection of $R_f - V_0$ curves shifts to a lower value of V_0 when either C_{bulk} or θ is increased. The shift of the point of intersection can be explained by the rate of ion transport. The rate of ion transport is lowered by the rate of decrease in the electric potential, which occurs when the overlapping of double layer is significant and ions accumulate most neat the nanopore tip. However, if C_{bulk} and/or θ take a higher value, the distributions of the electric potential of three types of salt examined are essentially the same.

In Chapter 2, taking account of effects of pH-regulated nature of a cylindrical nanopore surface functionalized with polyelectrolyte (PE) brushes and the presence of electroosmotic flow, we investigate the influence of applying an extra pH gradient in addition to an electric field on the ionic transport in the nanopore. An interesting phenomenon is observed: when applied a sufficiently strong pH gradient, the nanopore



exhibits disparate conductance response to the applied potential bias, depending upon its sign. For negatively applied potential bias, the conductance increases appreciably with increasing applied potential bias; for positively applied potential bias, it becomes insensitive to the bias. This discrepancy lies in difference in response of the charge density of PE brushes to the applied potential bias. We also demonstrate ion current rectification (ICR) in cylindrical nanopore. For a fixed strength of pH gradient, the ICR factor measuring the degree of ICR of the nanopore can be tuned by the applied potential bias. A rectification inversion is observed when the applied potential bias is ca. ± 0.3 V. The ICR behavior of the nanopore depends on dominance of either the applied pH gradient or charge density of PE brushes. For a moderate pH gradient strength, rectification inversion can also be observed when the grafting density of the PE brushes is raised. This study reveals that ionic transport in the nanopore can be influenced significantly by the applied pH gradient. Together with the key factors including nanopore geometry and the way to modify nanopore surface, we hypothesize that applying such a gradient can improve ICR performance of nanopores.